



**HAL**  
open science

## Molecular determinants of MED1 interaction with the DNA bound VDR–RXR heterodimer

Y Belorusova Anna, Maxime Bourguet, Steve Hessmann, Sandra Chalhoub, Bruno Kieffer, Sarah Cianférani, Natacha Rochel

► **To cite this version:**

Y Belorusova Anna, Maxime Bourguet, Steve Hessmann, Sandra Chalhoub, Bruno Kieffer, et al.. Molecular determinants of MED1 interaction with the DNA bound VDR–RXR heterodimer. *Nucleic Acids Research*, 2020, 10.1093/nar/gkaa775 . hal-02962412

**HAL Id: hal-02962412**

**<https://hal.science/hal-02962412>**

Submitted on 9 Oct 2020

**HAL** is a multi-disciplinary open access archive for the deposit and dissemination of scientific research documents, whether they are published or not. The documents may come from teaching and research institutions in France or abroad, or from public or private research centers.

L'archive ouverte pluridisciplinaire **HAL**, est destinée au dépôt et à la diffusion de documents scientifiques de niveau recherche, publiés ou non, émanant des établissements d'enseignement et de recherche français ou étrangers, des laboratoires publics ou privés.

**Some supplementary files may need to be viewed online via your Referee Centre at <http://mc.manuscriptcentral.com/nar>.**

**Molecular determinants of MED1 interaction with the DNA bound VDR-RXR heterodimer**

Journal:	<i>Nucleic Acids Research</i>
Manuscript ID	NAR-02013-M-2020.R1
Manuscript Type:	1 Standard Manuscript
Key Words:	nuclear receptor, mediator coactivator, integrative structural biology

SCHOLARONE™  
Manuscripts

## Molecular determinants of MED1 interaction with the DNA bound VDR-RXR heterodimer

Anna Y. Belorusova<sup>1-4,#</sup>✉, Maxime Bourguet<sup>5,#</sup>, Steve Hessmann<sup>5</sup>, Sandra Chalhoub<sup>1-4</sup>, Bruno Kieffer<sup>1-4</sup>, Sarah Cianférani<sup>5</sup>, Natacha Rochel<sup>1-4</sup>✉

<sup>1</sup>Institut de Génétique et de Biologie Moléculaire et Cellulaire (IGBMC), Illkirch, France.

<sup>2</sup>Centre National de la Recherche Scientifique UMR7104, Illkirch, France.

<sup>3</sup>Institut National de la Santé et de la Recherche Médicale U1258, Illkirch, France.

<sup>4</sup>Université de Strasbourg, Illkirch, France.

<sup>5</sup>Laboratoire de Spectrométrie de Masse BioOrganique, Université de Strasbourg, CNRS UMR 7178, IPHC, Strasbourg, France

#Co-first authors

✉ Correspondence to [Anna Y. Belorusova \(anna.y.belorusova@gmail.com\)](mailto:anna.y.belorusova@gmail.com) or [Natacha Rochel \(rochel@igbmc.fr\)](mailto:rochel@igbmc.fr)

### Abbreviations

1,25D3, 1 $\alpha$ ,25-dihydroxyvitaminD3; 9cisRA, 9cis retinoic acid; VDR, vitamin D receptor; RXR, retinoid X receptor; TR, thyroid receptor; ER, estrogen receptor; NR, nuclear receptor; LBD, ligand binding domain; DBD, DNA binding domain; NTD, N-terminal domain; RID, receptor-interacting domain; SRC, steroid receptor coactivator; AF, activation function; H, helix; NPPA, Natriuretic peptides A; VDRE, vitamin d response element; DR3, direct repeat separated by 3 nucleotides; SAXS, small angle X-ray scattering; MS, mass spectrometry; HDX-MS, hydrogen-deuterium exchange mass spectrometry; XL-MS, crosslinking mass spectrometry; cryoEM, cryo-electron microscopy; SEC, size exclusion chromatography; MALLS, multi-angle laser light scattering;  $R_g$ , gyration radius;  $D_{max}$ , maximal dimension; RFU, uptake relative fraction.

### Abstract

The MED1 subunit of the Mediator complex is an essential coactivator of nuclear receptor-mediated transcriptional activation. While structural requirements for ligand-dependent binding of classical coactivator motifs of MED1 to numerous nuclear receptor ligand-binding domains have been fully elucidated, the recognition of the full-length or truncated coactivator by full nuclear receptor complexes remain unknown. Here we present structural details of the

1  
2 interaction between a large part of MED1 comprising its structured N-terminal and the flexible  
3 receptor-interacting domains and the mutual heterodimer of the vitamin D receptor (VDR) and  
4 the retinoid X receptor (RXR) bound to their cognate DNA response element. Using a combination  
5 of structural and biophysical methods we show that the ligand-dependent interaction between  
6 VDR and the second coactivator motif of MED1 is crucial for complex formation and we identify  
7 additional, previously unseen, interaction details. In particular, we identified RXR regions  
8 involved in the interaction with the structured N-terminal domain of MED1, as well as VDR  
9 regions outside the classical coactivator binding cleft affected by coactivator recruitment. These  
10 findings highlight important roles of each receptor within the heterodimer in selective  
11 recognition of MED1 and contribute to our understanding of the nuclear receptor-coregulator  
12 complexes.  
13  
14  
15  
16  
17  
18  
19  
20  
21  
22  
23  
24  
25

## 26 **Introduction**

27 Nuclear receptor (NR) superfamily of ligand-regulated transcription factors activate or  
28 repress gene expression by recruiting coactivators, corepressors, chromatin remodelers and the  
29 general transcriptional machinery to the target genes (reviewed in (1,2)). Among classical NR  
30 coactivators is Mediator, an evolutionary conserved multi-protein complex facilitating multiple  
31 stages of gene expression, notably the chromatin remodeling and pre-initiation complex  
32 formation (reviewed in (3-5)). It was discovered as a group of factors needed for the yeast RNA  
33 polymerase II activity (6,7), and subsequently various mammalian Mediator subcomplexes have  
34 been isolated through association with NRs, such as TRAP complex associated with thyroid  
35 receptor (TR), (8) and DRIP complex associated with vitamin D receptor (VDR) (9). Other similar  
36 complexes included activator-recruited cofactor ARC (10), mammalian mediator (11),  
37 mammalian Srb/Mediator complex (12), PC2 (13) and CRSP (14). Mediator is involved in strong  
38 ligand-dependent interaction with NRs primarily via its largest subunit 1 (MED1) (15-22),  
39 although for some NRs the interaction can include other Mediator subunits and alternative  
40 cofactors (23-27).  
41  
42  
43  
44  
45  
46  
47  
48  
49  
50  
51  
52

53 As a classical NR-binding target, MED1 contains two LXXLL motifs, also called NR-boxes,  
54 localized in a central disordered receptor-interacting domain (RID). Binding of the coactivator  
55 LXXLL motifs to the activation function 2 (AF-2) of the receptor ligand-binding domain (LBD) has  
56 been extensively characterized by structural studies (28-30). Leucines from the coactivator LXXLL  
57  
58  
59  
60

1 motif are buried in the hydrophobic groove of the AF-2 surface formed by hydrophobic residues  
2 from helices H3, H4 and H12 of the LBD, and the NR box is locked by a charge clamp formed by a  
3 lysine on the NR H3 and a glutamate on H12. The two MED1 LXXLL motifs bind to NRs with  
4 different specificity: steroid hormone receptors preferentially bind to the first LXXLL motif,  
5 whereas non-steroid hormone receptors, such as TR and VDR, strongly interact with the second  
6 LXXLL motif (15,31,32).  
7  
8  
9  
10  
11  
12

13 Mediator-dependent mechanisms of NR regulation by MED1 include looping of enhancers  
14 to transcription start sites via an assembly process involving transcription factors, cohesin and  
15 non-coding RNAs (33-37); directly linking chromatin remodeling and the pre-initiation complex  
16 formation (24,25); or repression of transcription through the core Mediator-associated CDK8  
17 kinase module (reviewed in (38)). At the same time, some regulatory roles of MED1 could be  
18 Mediator-independent as it can be recruited to NRs independently from the other Mediator  
19 subunits, promoting the association with the Mediator core in a second step. Occupancies of  
20 MED1 and NRs on the genome sites are highly correlated (35,39) and MED1 levels are highly  
21 elevated on super-enhancers in embryonic stem cells and in cancer cells where NRs act as master  
22 regulators (40,41). Recent studies showed that intrinsically disordered regions of MED1 can form  
23 phase-separated droplets that compartmentalize and concentrate transcriptional regulators  
24 (42).  
25  
26  
27  
28  
29  
30  
31  
32  
33  
34

35 MED1 has been shown to be essential for various biological functions of large number of  
36 NRs (reviewed in (38)). Due to its important role in human physiology, it has been suggested as  
37 a possible target for several disorders, such as metabolic syndrome (43), fatty liver (44) and  
38 several types of cancer, including breast and prostate cancers (reviewed in (45)).  
39  
40  
41

42 Despite essential role and high therapeutic potential of MED1, no atomic structural data is  
43 available for this protein or its homologs. Furthermore, while much has been discovered about  
44 the Mediator complex and its association with transcriptional machinery, the mechanistic details  
45 of how MED1 bridges the Polymerase II to NRs are far less understood. Most of the structural  
46 investigations on NR-MED1 association, similarly to analogous coregulator complexes, are still  
47 limited to the recognition of LXXLL-peptides or short RIDs by NRs (46-48). Recent advances in  
48 single particle cryo-electron microscopy (cryoEM) allowed the structural characterization of the  
49 full-length estrogen receptor alpha/p160/p300 coactivator complexes (49,50). However, the  
50 detailed mechanism of how NRs trigger the formation of big regulatory complexes that directly  
51 alter the transcriptional rate has not yet been fully elucidated and remains challenging due to the  
52  
53  
54  
55  
56  
57  
58  
59  
60

1  
2 presence of large intrinsically disordered regions in the coactivators proteins and the associated  
3 flexibility of the complexes.  
4

5 To provide structural insights into the mechanism of the NR-MED1 specific association, in  
6 the present study we investigated the complex formed between a large fragment of the  
7 coactivator MED1 comprising its structured N-terminal region and the RID encompassing two  
8 LXXLL motifs and the full NR heterodimer formed by VDR and the retinoid X receptor (RXR). We  
9 combined structural methods including small angle X-ray scattering (SAXS), NMR, hydrogen-  
10 deuterium exchange coupled to mass spectrometry (HDX-MS), crosslinking mass spectrometry  
11 (XL-MS) as well as biophysical methods to characterize the MED1 recruitment by the receptor  
12 heterodimer and to get structural details of this assembly. We show that one molecule of MED1  
13 is recruited by the VDR-RXR heterodimer and confirm primary role of the VDR AF-2 interaction  
14 with the second LXXLL motif of MED1 in complex formation. We demonstrate that the RXR AF-2  
15 is not essential for the MED1 recruitment, however is affected upon MED1 binding. We also  
16 identify other RXR regions, as well as VDR regions outside the AF-2, which are included in the  
17 interaction and could be important for reaching the coactivator selectivity by VDR-RXR. Novel  
18 structural information on the NR-MED1 complex presented in this work is essential to understand  
19 the molecular organization and the interaction networks between complexes of such type.  
20  
21  
22  
23  
24  
25  
26  
27  
28  
29  
30  
31  
32  
33  
34

### 35 **Material and Methods.**

36 **Compounds.** 1 $\alpha$ ,25-dihydroxyvitaminD3 (1,25D3) and 9cis retinoic acid (9cisRA) were purchased  
37 from Sigma. The *rat Nppa* single strands DNAs (5'-AGAGGTCATGAAGGACATT-3' and  
38 5'-AATGTCCTTCATGACCTCT-3') were purchased from Sigma Aldrich and annealed. The MED1 NR2  
39 peptide (NHPMLMNLLKDN) was synthesized by Pascal Eberling (IGBMC peptide synthesis  
40 common facility).  
41  
42  
43  
44  
45

46 **Biochemistry.** In all experiments, human proteins (HsVDR and HsRXR $\alpha$ ) were used to form the  
47 VDR-RXR $\alpha$  complexes, except for surface plasmon resonance experiment where human VDR and  
48 mouse RXR $\alpha$  were used to form the complexes.  
49

50 cDNAs encoding full-length HsVDR (1-427), HsVDR $\Delta$ 166-216(1-427,  $\Delta$ 166-216) and HsVDR $\Delta$ H12  
51 (1-415) cloned into the pET28b vector were used to generate the N-terminal His-tagged proteins.  
52 HsRXR $\alpha$  $\Delta$ NTD (130-462), MmRXR $\alpha$  $\Delta$ NTD (132-467), MmRXR $\alpha$  $\Delta$ NTD $\Delta$ H12 (132-449),  
53 MmRXR $\alpha$  $\Delta$ NTD K289A,E458A cloned into pET15b, were expressed as N-terminal His-tagged  
54  
55  
56  
57  
58  
59  
60

1 proteins. Recombinant proteins were produced in Escherichia coli BL21 DE3 after induction with  
2 1 mM IPTG (OD600 ~ 0.7) at 23 °C for 4 hours. Soluble proteins were purified using  
3 chromatography column (HisTrap FF crude, 17-5286-01, GE) followed by size exclusion  
4 chromatography (SEC) on HiLoad Superdex 200 (28-9893-35 GE) equilibrated in 20 mM Tris-HCl,  
5 pH 8.0, 250 mM NaCl, 5% glycerol, 2 mM CHAPS and 1 mM TCEP. Full-length HsVDR and  
6 HsRXR $\alpha$  $\Delta$ NTD were mixed in stoichiometric amounts and purified by size exclusion  
7 chromatography (HiLoad Superdex 200, 28-9893-35, GE) equilibrated in 20 mM Tris-HCl, pH 8.0,  
8 200 mM NaCl, 5% glycerol, 2 mM CHAPS and 1 mM TCEP. Ligands (1,25D3 and 9cisRA) were  
9 added to the stoichiometric heterodimer and *rat NPPA* DR3 was mixed in a 1.1 equivalent ratio.  
10 The DNA complex was further purified by Size Exclusion Chromatography (SEC) in 20 mM Tris pH  
11 8.0, 75 mM NaCl, 75 mM KCl, 2 mM CHAPS, 5% Glycerol, 4 mM MgSO<sub>4</sub>, 1 mM TCEP. A cDNA  
12 encoding truncated human MED1 (50-660) cloned into pBacHW, pFastBac-1 (Invitrogen)  
13 baculovirus transfer vector adapted for Gateway, was used to produce HsMED1 proteins with N-  
14 terminal His-tag. Sf9 cells were infected with recombinant baculovirus at a multiplicity of  
15 infection equal 5 and cultured in TNM-FH supplemented with 10% FCS and 50 mg/ml gentamycin at  
16 27°C for 48 h. Cells were harvested by centrifugation (1,000 g for 15 min) and cell pellets were  
17 stored at -20°C prior purification. Soluble protein was purified using batch/gravity-flow affinity  
18 chromatography (cComplete, Roche). MED1 (50-660) was eluted by 250 mM Imidazole in binding  
19 buffer. Following the His-tag removal by Thrombin cleavage, the protein was further purified by  
20 SEC on HiLoad Superdex 200 (28-9893-35 GE) equilibrated in 20 mM Tris-HCl, pH 8.0, 250 mM  
21 NaCl, 5% glycerol, 2 mM CHAPS and 1 mM TCEP.

22 The proteins were concentrated to 3-6 mg/ml with an Amicon Ultra 30 kDa MWCO. Purity and  
23 homogeneity of all proteins were assessed by SDS and Native PAGE.

#### 24 **Gel retardation in TBE**

25 6% polyacrylamide gel was used to examine the migration of DNA-bound complexes and MED1.  
26 The samples were loaded onto the polyacrylamide gel, placed in a Bio-Rad chamber for gels and  
27 ran with constant current of 6 mA for 3 hours at 4°C in TBE migration buffer. Gels were revealed  
28 by Coomassie staining.

#### 29 **Small angle x-ray scattering**

1  
2 Synchrotron X-ray data were collected on a Pilatus 1M detector at the ESRF beamline BM29 (51).  
3  
4 100  $\mu\text{L}$  of VDR-RXR $\Delta$ NTD-DR3, MED1 (50-660) and their complex at concentrations 8.5 - 10 mg  
5  
6  $\text{mL}^{-1}$  in 25 mM HEPES pH 7.5, 150 mM NaCl, 5% Glycerol, 2 mM  $\text{MgCl}_2$ , 2 mM TCEP were loaded  
7  
8 onto a GE Healthcare Superdex 200 10/300 column (equilibrated in the same buffer) at a flow  
9  
10 rate of 1  $\text{mL}\cdot\text{min}^{-1}$ . A scattering profile was integrated every second. Frames were selected based  
11  
12 on the examination of the SEC profile together with the calculated  $R_g$  and  $D_{\text{max}}$  values. The SAXS  
13  
14 data were averaged and processed by standard procedures using PRIMUS (52). The forward  
15  
16 scattering  $I(0)$  and the radii of gyration  $R_g$  were evaluated using the Guinier approximation  
17  
18 assuming that at very small angles ( $s < 1.3/R_g$ ) the intensity is represented as  $I(s) = I(0) \exp(-$   
19  
20  $(sR_g)^2/3)$ . These parameters were also computed from the entire scattering pattern using the  
21  
22 indirect transform package GNOM (53) which also provides the maximum dimension of the  
23  
24 particle  $D_{\text{max}}$  and the distance distribution function  $p(r)$ . The program SASREF (54) was employed  
25  
26 for molecular rigid body modeling of the VDR-RXR-DNA complex, based on SAXS and cryoEM  
27  
28 structures (48,55). The final fits of the model scattering to the experimental data were computed  
29  
30 using CRY SOL (56).

### 31 **Size exclusion chromatography coupled with multi-angle laser light scattering**

32 The molecular weight and homogeneity of the sample was checked using a SEC column coupled  
33  
34 with multi-angle laser light scattering (MALLS) Dawn DSP detector (Wyatt Technology, Santa  
35  
36 Barbara, CA, USA). A GE Healthcare Superdex 200 10/300 analytical column was pre-equilibrated  
37  
38 with the sample buffer, 25 mM HEPES pH 7.5, 150 mM NaCl, 5% Glycerol, 2 mM  $\text{MgCl}_2$ , 2 mM  
39  
40 TCEP. The system was operated at 20°C, with a flow rate of 0.75 ml/min.

### 41 **Analytical ultracentrifugation**

42 Sedimentation velocity experiments were performed at 4°C in 25 mM Tris-HCl pH 8.0, 100 mM  
43  
44 NaCl, 2% Glycerol, 1 mM CHAPS, 2 mM  $\text{MgCl}_2$ , 1 mM TCEP using Beckman Coulter Proteome Lab  
45  
46 XL-I analytical ultracentrifuge and the 8-hole Beckman An-50Ti rotor. Sedimentation at 50,000  
47  
48 rpm was monitored by absorbance at 280 nm with boundaries measured each 7 min. MED1 (50-  
49  
50 660) at constant concentration (6  $\mu\text{M}$ ) was titrated by VDR-RXR-DNA; tested  
51  
52 coactivator:heterodimer ratios varied from 1:0.5 to 1:2.7. Density and viscosity of the used buffer  
53  
54 were calculated using SEDNTERP software (<http://sednterp.unh.edu/>) and used for the data  
55  
56 correction. Using nonlinear least-squares analysis with SEDPHAT (57), collected datasets were  
57  
58 fitted using single site hetero-association model.  
59  
60

## Hydrogen deuterium exchange coupled to mass spectrometry

HDX experiments of VDR-RXR $\Delta$ NTD-DNA complex were carried out with and without 2 molar excess of NR2 motif in 20 mM Tris pH 8.0, 75 mM NaCl, 75 mM KCl, 2 mM CHAPS, 5% glycerol, 4 mM MgSO<sub>4</sub>, 1 mM TCEP. The same buffer was used for VDR-RXR-DNA-MED1(50-660) complex HDX experiment. Preparation and injection of the samples were automatically conducted using a LEAP HDX Automation Manager (Waters), while chromatography was carried out on an Acquity UPLC system with HDX technology (Waters, Manchester, UK). Samples were incubated at different deuteration times (0, 0.5, 2, 10 and 30 min) in 95% of deuterated buffer (20 mM Tris pD 8.0, 75 mM NaCl, 75 mM KCl, 4 mM MgSO<sub>4</sub>, 1 mM TCEP) before quenching the exchange by adding a 150 mM glycine pH 2.4, 2 M GdHCl, 4 mM MgSO<sub>4</sub>, 1 mM TCEP buffer at 1 °C during 30 s. Digestion of samples (between 20 and 50 pmoles injections) was then performed through a pepsin-immobilized cartridge in 0.1% aqueous formic acid solution at a 200  $\mu$ l/min. Generated Peptides were then trapped on a UPLC pre-column (ACQUITY UPLC BEH C18 VanGuard pre-column, 2.1 mm I.D.  $\times$  5 mm, 1.7  $\mu$ M particle diameter, Waters) and separated on UPLC column (ACQUITY UPLC BEH C18, 1.0 mm I.D.  $\times$  100 mm, 1.7  $\mu$ M particle diameter, Waters) at 0 °C. Mass spectrometry analyses were acquired with Synapt G2Si HDMS (Waters) with electrospray ionization, using data-independent acquisition mode (MS<sup>E</sup>) over an  $m/z$  range of 50–2000 and 100 fmol/ $\mu$ l Glu-FibrinoPeptide solution as lock-mass correction and calibration. Analyses were performed with the following parameters: capillary voltage, 3 kV; sampling cone voltage, 40 V; source temperature, 80°C; desolvation gas, 150°C and 600 L.h<sup>-1</sup>; scan time, 0.3 s; trap collision energy ramp, 15 to 40 eV. HDX experiments were realized in triplicate for each time point. Peptide identification was performed using ProteinLynx Global Server 2.5.3 (Waters) with a home-made protein sequence library containing VDR, RXR and MED1(50-660) sequences, with peptide and fragment tolerances set automatically by PLGS, and oxidized methionine set as variable modification. Deuterium uptakes for all identified peptides were then filtered and validated manually using DynamX 3.0 (Waters) as follows: only peptides identified in all replicates were kept with only one charge state with a minimum fragment of 0.2 per amino acid, a minimum intensity at 10<sup>3</sup>, a length between 5 and 30 residues and a file threshold of 3. Deuterium uptakes were not corrected and are reported as relative. HDX-MS results were statistically validated using Mixed-Effects Model for HDX experiments (MEMHDX, (58)) where statistical significance thresholds were set to 0.01. HDX results were exported on VDR-RXR SAXS model using PyMOL

1  
2 ([www.pymol.org](http://www.pymol.org)). HDX-MS data have been deposited to the ProteomeXchange Consortium via  
3  
4 the PRIDE (59) partner repository with the dataset identifier PXD019530.

### 5 **Chemical crosslinking coupled to mass spectrometry**

6  
7 Crosslinking reactions were conducted with 25  $\mu$ M protein solutions in 20 mM HEPES pH 8.0, 75  
8 mM NaCl, 75 mM KCl, 4 mM MgSO<sub>4</sub>, 1 mM TCEP Freshly prepared 10 mM stock solution of DSBU  
9 and C2-arm version of DSBU in DMSO (CF Plus Chemicals s.r.o., Czech Republic) were added in  
10 50-, 100- and 200-fold molar excess. Crosslinking reactions were conducted during 45 min at  
11 room temperature and further quenched during 20 min using NH<sub>4</sub>HCO<sub>3</sub> to a final concentration  
12 of 20 mM final. Disulfide reduction was next performed by incubating the crosslinked complex  
13 solution with 5 mM DTT for 30 min at 60°C, followed by alkylation with 15 mM IAA for 30 min in  
14 the dark. Then trypsin (Promega, Madison, USA) was added in 1:50 enzyme: substrate ratio.  
15 Samples were incubated overnight at 37°C. Digestion was quenched with 1% formic acid.  
16 Peptides were cleaned up using SPE cartridges and samples were concentrated in a SpeedVac  
17 concentrator before LC/MS/MS analysis. NanoLC-MS/MS analyses were performed using a  
18 nanoAcquity UPLC (Waters, Milford, USA) coupled to the Q-Exactive Plus Orbitrap mass  
19 spectrometer (Thermo Scientific, Bremen, Germany) Nanospray Flex™ Ion source. The samples  
20 were trapped on a nanoACQUITY UPLC precolumn (C18, 180  $\mu$ m x 20 mm, 5  $\mu$ m particle size),  
21 and the peptides were separated on a nanoACQUITY UPLC column (C18, 75 $\mu$ m x 250 mm with  
22 1.7  $\mu$ m particle size, Waters, Milford, USA) maintained at 60°C. The samples were first injected  
23 with a 285 min gradient and a flow rate of 450 nL/min. The Q-Exactive Plus Orbitrap source  
24 temperature was set to 250°C and spray voltage to 1.8kV. Full scan MS spectra (300-1800 m/z)  
25 were acquired in positive mode at a resolution of 140 000, a maximum injection time of 50 ms  
26 and an AGC target value of  $3 \times 10^6$  charges, with lock-mass option being enabled (polysiloxane  
27 ion from ambient air at 445.12 m/z). The 10 most intense multiply charged ions per full scan  
28 (charge states >2) were isolated using a 2 m/z window and fragmented using higher energy  
29 collisional dissociation (30 normalized collision energy,  $\pm 3\%$ ). MS/MS spectra were acquired with  
30 a resolution of 35 000, a maximum injection time of 100 ms, an AGC target value of  $1 \times 10^5$  and  
31 dynamic exclusion was set to 60 sec. The system was fully controlled by XCalibur software  
32 v3.0.63, 2013 (Thermo Scientific) and NanoAcquity UPLC console v1.51.3347 (Waters). Raw data  
33 collected were processed and converted into .mgf format. The MS/MS data were analyzed using  
34 MeroX software version 1.6.6 (60). Mass tolerance of 5 ppm for precursor ions and 10 ppm for  
35 product ions were applied. A 5% FDR cut-off and a signal-to-noise  $\geq 2$  were applied. For both  
36  
37  
38  
39  
40  
41  
42  
43  
44  
45  
46  
47  
48  
49  
50  
51  
52  
53  
54  
55  
56  
57  
58  
59  
60

1  
2 crosslinkers, Lys and Arg were considered as protease cleavage sites with a maximum of three  
3 missed cleavages. Carbamidomethylation of cysteine was set as fixed and oxidation of  
4 methionine as variable modifications (max. mod. 2). Primary amino groups (Lys side chains and  
5 N-termini) as well as primary hydroxyl groups (Ser, Thr and Tyr side chains) were considered as  
6 crosslinking sites. The cRap database was used in combination with the reporter ion scan event  
7 (RISE) mode on. Crosslinks composed of consecutive amino acid sequences were not considered.  
8 Each crosslinked product automatically annotated with MeroX was manually validated. Finally,  
9 PyMOL software ([www.pymol.org](http://www.pymol.org)) was used to calculate the C $\alpha$ -C $\alpha$  distance of each validated  
10 linkage sites. The XL-MS data set has been deposited to the ProteomeXchange Consortium via  
11 the PRIDE (59) partner repository with the dataset identifier PXD019530.

## 20 **NMR**

21 NMR experiments were recorded at 280 K on an Avance III Bruker 700 MHz equipped with a z-  
22 gradient TCI cryoprobe. NMR samples consisted of 65  $\mu$ M solution of  $^{15}$ N labelled VDR, either  
23 full-length or VDR $\Delta$ 166-216, alone or in complex with 1,25D3, liganded RXR $\Delta$ NTD and DNA in  
24 buffer containing 25 mM citrate, pH 6.3, 100 mM NaCl, 5% Glycerol, 2 mM MgCl<sub>2</sub> and 1 mM TCEP  
25 in a 3 mm NMR tube. Interaction with MED1 was studied by adding equimolar amounts of MED1  
26 (50-660) protein to the VDR-RXR $\Delta$ NTD-DNA and VDR $\Delta$ 166-216-RXR $\Delta$ NTD-DNA complexes, where  
27 VDR was full-length or devoid of the LBD insertion region, respectively.  $^1$ H- $^{15}$ N HSQC were  
28 recorded using WATERGATE solvent suppression pulse sequence from the Bruker standard  
29 library with a total acquisition time of four hours.

## 38 **Surface Plasmon Resonance**

40 Measurements were performed by Biacore T100 sensitivity enhanced T200 equipment (GE  
41 Healthcare) using CM5 series S sensor chip (GE) (29-1496-03). MED1(50-660) was immobilized  
42 on the chip surface using standard amino-coupling protocol in 10 mM Na-acetate buffer pH 5.5.  
43 The resulting immobilized MED1 was in the range of 100-200 response unit. The running buffer  
44 was 50 mM Hepes pH 7.5, 400 mM NaCl, 1 mM TCEP, 0.005% Tween 20 and for regeneration 1M  
45 sodium chloride solution was used. Interactions of the MED1 with fully liganded VDR-RXR wild  
46 type, VDR $\Delta$ H12-RXR, VDR-RXR AF-2 mutant and VDR-RXR  $\Delta$ H12 were analyzed in the manner of  
47 dose response using twofold dilution series of VDR-RXR ranging from 0.01 to 8  $\mu$ M. The  
48 association phase was 120 s and the dissociation phase was 120 s. After subtracting the reference  
49  
50  
51  
52  
53  
54  
55  
56  
57  
58  
59  
60

1  
2 and buffer signal, the data were fit to a steady state binding model using the Biacore T200  
3 Evaluation software (GE Healthcare).  
4  
5  
6

## 7 **Results**

### 8 ***Binding of MED1 N-terminal domain to VDR-RXR***

9  
10  
11 Previous structural studies uncovered details of the VDR LBD interaction with the second  
12 LXXLL motif of MED1 (NR2 motif, residues 645-649) (32,61) (Supplementary Figure 1a), and we  
13 have previously shown that the MED1 RID binds to the VDR-RXR heterodimer asymmetrically and  
14 remains flexible (47). To gain further insights into specific association between VDR-RXR and  
15 MED1, we investigated the binding of the receptor heterodimer to a larger fragment of the  
16 coactivator. Based on the disorder prediction for MED1 (Supplementary Figure 1a,b), we selected  
17 a protein construct spanning from residues 50 to 660 encompassing the structured N-terminus  
18 and RID, as previous studies suggested that first 570 residues of MED1 are sufficient for its  
19 incorporation into the Mediator (62).  
20  
21  
22  
23  
24  
25  
26

27 We investigated how purified MED1 (50-660) fragment interacts with the heterodimer  
28 formed by the full-length VDR and the RXR $\alpha$  lacking the flexible N-terminal domain (NTD), named  
29 hereafter VDR-RXR, and associated with a DR3-type vitamin D response element (VDRE). To  
30 stabilize the VDR-RXR heterodimer, we selected the VDRE from *rat Nppa* gene alternatively  
31 named *rat ANF1* gene (63) displaying a low nanomolar affinity for VDR-RXR complex  
32 (Supplementary Figure 2a). In addition, we showed by a transactivation assay in HEK 293 cells  
33 that the luciferase gene under control of the *rat Nppa* promoter is activated by the VDR natural  
34 ligand, 1,25D3, at nanomolar concentrations (Supplementary Figure 2b). The complex was  
35 formed by an overnight incubation of the purified VDR-RXR bound with their cognate ligands,  
36 1,25D3 and 9cisRA, and the purified MED1 fragment. The presence of the two ligands in the VDR-  
37 RXR complex was confirmed by native **electrospray ionization mass spectrometry** (data not  
38 shown). The complex formation with MED1 was observed by gel retardation assay  
39 (Supplementary Figure 2c) and size-exclusion chromatography (SEC), where the newly formed  
40 high molecular weight complex could immediately be detected as a new specimen appearing on  
41 the elution profile before the MED1 (68 kDa) and the VDR-RXR (86 kDa) (Supplementary Figure  
42 2d-e). The molecular weight of the complex as measured by multi-angle light scattering was in  
43 close agreement with the respective calculated molecular weight of complex where MED1 binds  
44 to VDR-RXR in a 1:1 stoichiometry (Figure 1a). The binding mode of MED1 to VDR-RXR-DNA was  
45  
46  
47  
48  
49  
50  
51  
52  
53  
54  
55  
56  
57  
58  
59  
60

1 further analyzed by analytical ultracentrifugation in sedimentation velocity mode  
2 (Supplementary Figure 3). The distribution of sedimentation coefficients  $c(s)$  (Figure 1b)  
3 confirmed the formation of the complex between the MED1 and VDR-RXR-DNA and the complex  
4 stoichiometry. Interestingly, the  $c(s)$  peak shifted in a concentration-dependent way indicating  
5 fast kinetics of the interaction ( $k_{\text{off}} > 10^{-2} \text{ s}^{-1}$ ).  
6  
7  
8  
9

10 All together, the biophysical data indicates that only one MED1 molecule binds to the  
11 liganded VDR-RXR heterodimer and we show that the process of the protein association-  
12 dissociation is dynamic and the complex is rather transient.  
13  
14  
15  
16  
17

### 18 **Topology of the MED1-VDR-RXR-DNA complex**

19 To gain better insights into the overall structures of the multi-modular VDR-RXR-DNA and  
20 VDR-RXR-DNA-MED1 complexes, we determined their solution structures using SAXS. SAXS data  
21 were collected from samples of MED1, liganded VDR-RXR-DNA and liganded VDR-RXR-DNA-  
22 MED1 using on-line SEC (SEC-SAXS) (Supplementary Figure 4). The SAXS profiles are shown in  
23 Figure 2a-b and Supplementary Figure 5 and the structural parameters including the radius of  
24 gyration,  $R_g$ , and the maximum particle dimension,  $D_{\text{max}}$ , are reported in Table 1. For MED1 alone,  
25 the Kratky plot representation of MED1 scattering data (Supplementary Figure 5c) suggests that  
26 the fragment is globular and has one core with flexible parts/linkers. The structural parameters  
27 values for VDR-RXR-DNA are slightly larger than those previously determined for the related  
28 VDR $\Delta$ -RXR-DNA complex where VDR-specific insertion localized between H1 and H3 was  
29 truncated (47). Binding of MED1 to VDR-RXR-DNA increases the average size of the complex but  
30 does not induce a large change in the overall SAXS profile: similar distinctive 'humps' around 1  
31 nm<sup>-1</sup> are observed in the SAXS curves for VDR-RXR-DNA alone and in complex with MED1 (Figure  
32 2a,c). The probability distribution of real-space scattering pair distances, or  $p(r)$  profiles, reveals  
33 a similar shoulder around 60-80 Å for both complexes (Figure 2b). This indicates that the shape  
34 of the VDR-RXR-DNA in complex with MED1 remains similar to that of the DNA-bound  
35 heterodimer, where the DNA binding domains (DBDs) are spatially separated from the LBDs.  
36 Comparison of the most representative *ab initio* models of VDR-RXR-DNA and VDR-RXR-DNA-  
37 MED1 complexes obtained with DAMMIN (64) reveals overall shape similarities with two  
38 distinguishable domains (Figure 2c) indicating no major conformational change of the DNA-  
39 bound heterodimer upon MED1 interaction. For the coactivator complex, an additional electron  
40 density at the region occupied by both LBDs is visible indicating that the globular domain of MED1  
41  
42  
43  
44  
45  
46  
47  
48  
49  
50  
51  
52  
53  
54  
55  
56  
57  
58  
59  
60

1  
2 is likely located on “top” of the heterodimer and is interacting with the VDR-RXR LBD heterodimer  
3  
4 via an extensive area.  
5  
6

### 7 ***VDR insertion domain modulates MED1 interaction with the VDR-RXR heterodimer***

9  
10 Whereas the *ab initio* SAXS envelope visualizes the overall shapes, the rigid-body  
11 refinement provides a model that reflects the overall distribution of conformers in solution and  
12 is not restricted to a particular low-energy conformation of the macromolecules. For the VDR-  
13 RXR-DNA complex, we built an ensemble of SAXS compatible models (Figure 2d) using the crystal  
14 structures of the DNA and ligand binding domains of VDR and RXR (65-67) with missing regions  
15 (VDR NTD, hinges, VDR’s insertion) modeled as dummy residues. The insertion region in VDR LBD  
16 is a 50 amino acid domain specific for VDR and poorly conserved between VDR family members  
17 and disordered in context of the isolated LBD (68). In the obtained refined models of VDR-RXR-  
18 DNA (Figure 2a) it occupies a defined region of space similar in all refined models suggesting that  
19 the insertion domain although possibly flexible is not totally disordered. Modelling also suggests  
20 that the VDR NTD (residues 1-23) is rather flexible, adopting various extended conformation in  
21 solution and not interacting with the DNA.  
22  
23  
24  
25  
26  
27  
28  
29  
30

31  
32 The best refined model docked into the SAXS envelope of VDR-RXR-DNA-MED1 (Figure  
33 2e) reveals a proximity and possible overlap of the areas occupied by the VDR insertion domain  
34 and MED1, thus suggesting that this VDR region may be interacting with MED1. To further  
35 characterize the involvement of the disordered VDR insertion domain in MED1 association, a  
36 NMR analysis of N<sup>15</sup>-labelled VDR complexes was performed. As VDR exhibits two disordered  
37 regions, the short NTD and the insertion domain, we compared the <sup>1</sup>H-<sup>15</sup>N HSQCs recorded for  
38 DNA bound heterodimer where VDR was either full-length or truncated of its insertion domain,  
39 with or without addition of MED1. The size of the complexes filters out signals from folded  
40 regions leaving only amide resonances from disordered regions belonging to the NTD and  
41 insertion in full-length LBD (Figure 2f,g). The addition of MED1 to VDR-RXR-DNA complex led to  
42 the specific disappearance of a small number of cross peaks specifically found in the full-length  
43 VDR indicating that the disordered insertion is involved, either directly or indirectly, in the  
44 interaction with MED1.  
45  
46  
47  
48  
49  
50  
51  
52  
53  
54  
55

### 56 ***Roles of VDR and RXR AF-2 in association with MED1***

1  
2 To analyze the roles of the VDR and RXR AF-2 in interaction with MED1 (50-660) fragment,  
3 we mutated VDR and RXR and determined the impact of mutations on the association with MED1  
4 by surface plasmon resonance. MED1 fails to interact to VDR-RXR when VDR H12 is deleted, or  
5 in presence of VDR antagonist ligand (ZK168281) (69) (Figure 1c and Supplementary Figure 8),  
6 thus confirming that the main anchoring interaction are agonist-dependent and mediated  
7 through VDR AF-2, in agreement with previous studies showing that a synthetic peptide  
8 comprising classical NR-interacting LXXLL motif competes with MED1 for interaction with the VDR  
9 (70). In contrast, deletion of RXR H12 does not prevent MED1 binding to VDR-RXR-DNA. A slightly  
10 increased MED1 binding is observed for VDR-RXRDeltaH12. Mutations of RXR residues forming a  
11 charge clamp for proper orientation and binding of the LXXLL motif of the coactivator (71,72) has  
12 no effect on MED1 interaction.

13  
14 In addition, we investigated the impact of the binding of the peptide bearing the MED1  
15 NR2 motif (residues 645-649) on the VDR-RXR-DNA complex using HDX-MS. We observed that  
16 two regions of VDR corresponding to the NTD and the insertion domain exhibit fast H/D exchange  
17 rates (Supplementary Figure 6a) which is a typical phenomenon for highly flexible regions (73),  
18 thus supporting SAXS results. Similar fast HDX rates were also observed for several regions of RXR  
19 (Supplementary Figure 6b), encompassing the hinge region, helix H1, H2, the C-terminus of H3,  
20 H11, the C-terminus of H12, and the region after H12. The comparison of relative fractional  
21 uptakes (RFU) of VDR-RXR-DNA and VDR-RXR-DNA-MED1 NR2 motif revealed that mainly VDR  
22 region 411-419 spanning the C-terminus of H11n and the N-terminus of the helix H12 was  
23 protected from H/D exchange upon NR2 motif binding (Figure 3 and Supplementary Figure 7a).  
24 These results are in agreement with the crystal structures of VDR LBD complexes with coactivator  
25 peptides (74,75), highlighting the role of VDR AF-2 in its interaction with MED1 NR2 through H3,  
26 H4 and H12 helices. On the contrary, no significant differences were detected for RXR upon MED1  
27 NR2 motif binding (Figure 3 and Supplementary Figure 7b), supported by the low affinity of MED1  
28 NR2 for RXR (72,76). Taken together, our data show that the AF-2 of VDR but not RXR is directly  
29 involved in agonist-induced binding of MED1.

### 51 52 53 ***Effect of MED1 (50-660) binding on the VDR-RXR heterodimer***

54 We next performed HDX-MS experiments with the larger construct of MED1 to determine  
55 the effect of binding on both the coactivator and the VDR-RXR heterodimer.  
56  
57  
58  
59  
60

1  
2 HDX-MS of MED1 (50-660) fragment revealed that the protein is mostly structured  
3 (Supplementary Figure 9a), in agreement with the disorder prediction (Supplementary Figure  
4 9b). Several MED1 regions exhibit fast H/D exchange rates and can be characterized as highly  
5 flexible, including residues 61-74, 161-174, 191-201, 231-255, 276-296, 327-339 and 480-487  
6 which could correspond to flexible loops between the secondary structure elements  
7 (Supplementary Figure 9c). MED1 RID is also highly flexible, in agreement with our previous data  
8 (47).  
9

10  
11 We compared HDX-MS RFU values of VDR and RXR in VDR-RXR-DNA complex with those  
12 in VDR-RXR-DNA-MED1 (50-660) state to characterize their conformational dynamics upon MED1  
13 binding. As expected, C-terminus of H11n and N-terminus of H12 of VDR (protected upon MED1  
14 NR2 binding) were similarly affected upon MED1 (50-660) binding (Figure 3 and Supplementary  
15 Figure 10a). Additional regions of VDR were protected, including helices H3, the C-terminus of  
16 H5, H6, H7, H10 and H11. These regions are spatially close to the VDR AF-2 domain (Figure 3b),  
17 revealing a higher protection effect on this region upon MED1 (50-660) binding compared to the  
18 binding of MED1 NR2 motif.  
19

20  
21 Interestingly, several protected regions of RXR LBD were identified upon MED1 (50-660)  
22 binding, corresponding to helices H3, H5 and the  $\beta$ -strand, H11 and the N-terminus of H12 (Figure  
23 3 and Supplementary 10b). These regions are spatially close to each other and are located on  
24 “top” of the heterodimer LBDs supporting the SAXS models indicating that this region creates a  
25 large MED1 interaction surface. Of note, region 419-429 of RXR, covering helix H10 and  
26 comprising the heterodimerization interface, shows deprotection upon MED1 binding at shorter  
27 time points suggesting a conformational change leading to its higher flexibility (Figure 3b and  
28 Supplementary Figure 9b).  
29

30  
31 MED1 (50-660) is also protected upon formation of the complex with VDR-RXR-DNA  
32 (Supplementary Figure 11). Residues 243-255 of the structured N-terminal domain of MED1 are  
33 particularly protected upon VDR-RXR-DNA binding (Figure 3e). Other affected regions are 74-107,  
34 123-150, 191-201, 509-527 as well as regions 560-604, 636-645 and 649-657 situated within the  
35 unstructured part of MED1 comprising RID. Regions 560-604 and 636-645 encompass the first  
36 leucine residues of both NR boxes 1 and 2 of MED1 RID domain respectively (Leu604 and Leu645),  
37 suggesting a stabilization of both motifs upon NR binding.  
38

39  
40 All together, these results show that MED1 (50-660) binding affects extended regions  
41 within the liganded VDR-RXR LBD heterodimer, in contrast to the MED1 NR2 motif stabilizing  
42  
43  
44  
45  
46  
47  
48  
49  
50  
51  
52  
53  
54  
55  
56  
57  
58  
59  
60

solely the C-terminus of VDR. In addition to the VDR coactivator cleft and H12 strongly stabilized upon MED1 binding, several RXR regions including AF-2 and H5/ $\beta$ -strand are affected indicating role of RXR in establishing a specific association with the coactivator.

### ***Investigation of the interaction surface between MED1 and VDR-RXR heterodimer***

To determine molecular constraints and amino acids of VDR-RXR and MED1 located in close proximity, we next performed XL-MS on VDR-RXR-DNA-MED1 (50-660) complex using DSBU (spacer arm 12.5 Å) (77) and a C2-arm version of the DSBU (spacer arm 6.2 Å) (see material and methods). Both crosslinkers are MS-cleavable, allowing more confident MS/MS identification and validation thanks to the detection of characteristic doublet peaks along with the peptide backbone fragments (78). Both DSBU crosslinker versions target primary amines as well as hydroxyl groups and can bridge residues with  $\text{C}\alpha$ - $\text{C}\alpha$  distances up to 26-30 Å and 20-24 Å for DSBU and the C2-arm, respectively (79). We identified 42 intra- and inter-crosslinked peptides: 11 crosslinks intra-RXR, 12 intra-VDR, 6 intra-MED1, 12 inter-VDR-RXR and 1 inter-MED1-RXR (Figure 4 and Supplementary S12a). Twelve crosslinks involving VDR and RXR were found in the proximity to or within the DBDs when mapped on the VDR-RXR heterodimer model (55) and with a  $\text{C}\alpha$ - $\text{C}\alpha$  distance below the cut-off mentioned, increasing confidence in our XL-MS approach (Supplementary Figure 12b). Interestingly, an inter-protein crosslink involving Thr236 of MED1 and Lys321 of RXR was identified. Lys321 is located in the  $\beta$ -strand between H5 and H6 of RXR LBD (Figure 4b) on “top” of the LBD heterodimer and within the region protected from the H/D exchange upon MED1 binding correlating with the SAXS and HDX-MS results. Taken together, our data suggests that although RXR H12 is not required for MED1 recruitment, RXR LBD possesses an extensive surface directly interacting with MED1.

### **Discussion**

While structural requirements for ligand-dependent binding of classical coactivator motifs to NRs have been fully elucidated (reviewed in (80)), the molecular mechanism of co-activation remains poorly understood. In particular, studies providing structural insights into recognition of full-length or truncated coactivators by full NR complexes remain extremely scarce (47,49,50,81). Here, we describe novel structural data (Figure 5) on the complex formed between the agonist- and DNA-bound VDR-RXR heterodimer and a large fragment of the classical nuclear receptor coactivator MED1, an important regulator of VDR function (82). **In contrast to earlier**

1  
2 studies of the VDR-MED1 interactions where the isolated LBD of VDR or its truncated version  
3 were used (32,47,61), use of the functional full-length VDR-RXR complex allowed us to  
4 identify novel receptor regions involved in the coactivator recruitment.  
5  
6

7 MED1 interacts with NRs through a disordered RID domain that contains two LXXLL motifs  
8 (70). Early mutagenesis studies revealed that in case of the VDR-RXR heterodimer VDR binds with  
9 high affinity the second LXXLL motif of MED1 but not the NR1 box, and RXR shows only weak  
10 binding to both motifs (32,83,84). In addition, mutations in the VDR's charge clamp render VDR  
11 inactive, confirming that interaction with coactivators is crucial for its activity (85). Our results  
12 confirm that MED1 NR2-VDR interaction is driving the complex formation. However, by using a  
13 larger fragment of MED1, MED1 (50-660), we have also demonstrated that other VDR-RXR  
14 regions outside the VDR AF-2 as well as MED1 regions other than RID modulate the association  
15 and form an extended interaction surface.  
16  
17

18 Both LXXLL motifs of MED1, as well as proper spacing between the motifs, were reported  
19 to be required for optimal MED1 binding to DNA-bound VDR-RXR heterodimer (32). It was  
20 suggested that each LXXLL motif is recognized by VDR and RXR coactivator binding clefts  
21 simultaneously when the complex with MED1 is formed. In this case the 35 amino acid spacer  
22 between the two LXXLL motifs has to clasp around the LBDs as the coactivator binding sites are  
23 located on the opposite sites of the heterodimer. However, we have previously shown that the  
24 MED1 RID binds to the VDR-RXR heterodimer asymmetrically and remains flexible (47).  
25 Interestingly, in the present study, we observed the perturbation of both LXXLL motifs of MED1  
26 (50-660) upon formation of the complex with VDR-RXR, suggesting that while the NR1 box is not  
27 accommodated within the classical coactivator binding site, it could be either interacting with an  
28 alternative site of the receptors or stabilized allosterically. Similar observations have previously  
29 been made for the three NR boxes of the SRC-2 RID binding to PPARG-RXR (86). Alternative  
30 interaction with **androgen receptor** AF-1 was previously described for two noncanonical  $\alpha$ -helical  
31 motifs of MED1 located between residues 505 and 537 and in proximity to the NR box 1 (87).  
32  
33

34 Here we demonstrate that, in addition to RID, the structured N-terminal domain of MED1  
35 is also affected upon binding to VDR-RXR and is likely interacting with both VDR and RXR LBDs. In  
36 particular, MED1 region 243-255 is largely stabilized in the complex with the receptor  
37 heterodimer. Neighboring Thr236 of MED1 was identified within inter-MED1-RXR crosslink,  
38 suggesting that this MED1 region is in physical proximity to the RXR  $\beta$ -strand which, in turn, is  
39 also perturbed upon the interaction. As N-terminal region of MED1 is involved in important  
40  
41  
42  
43  
44  
45  
46  
47  
48  
49  
50  
51  
52  
53  
54  
55  
56  
57  
58  
59  
60

1  
2 downstream interactions such as incorporation into Mediator (62) and recruitment of alternative  
3 cofactors to enhancer-bound NRs (26), it is tempting to speculate that by creating an extended  
4 surface for MED1 accommodation and altering its conformation, RXR could be important for  
5 achieving optimal MED1-mediated transcription activation.  
6  
7

8  
9 Among other novel MED1-interacting regions within the VDR-RXR heterodimer is the  
10 flexible insertion domain in the VDR LBD located between H1 and H3. By using <sup>15</sup>N NMR, we show  
11 that it undergoes conformational changes upon interaction with MED1. This effect is not seen in  
12 the HDX-MS experiment; however the observed difference could be attributed to a different  
13 temporal resolution of the two methods. While the VDR insertion domain does not play a major  
14 role in receptor selectivity for 1,25D3 (70) nor bile acids (88), previously published data suggests  
15 that it has a functional role in regulation of VDR signaling. Several phosphorylations modulating  
16 VDR transcriptional activity, S182 and S208, have been identified within this region (89).  
17 Interestingly, S208 phosphorylation has previously been reported to enhance VDR interaction  
18 with MED1 but not with the SRC-1 coactivator (90,91).  
19  
20  
21  
22  
23  
24  
25  
26

27 In this study we used the full VDR-RXR heterodimer in agonist-bound form, where both  
28 VDR and RXR ligands were present. Hypothetically, each receptor can recruit a coactivator,  
29 however, we demonstrate that only one molecule of MED1 is recruited by the VDR-RXR  
30 heterodimer, suggesting that H12 of RXR is not essential for the complex formation. Indeed,  
31 truncation of RXR H12 and mutations in RXR charge clamp do not prevent MED1 interaction, and  
32 binding of a peptide comprising MED1 NR2 does not induce any change in RXR as seen by HDX-  
33 MS. However, using HDX-MS, we identified H3, H11 and the N-terminus of H12 comprising the  
34 AF-2 among RXR regions largely stabilized upon MED1 binding. The observed stabilization event  
35 could originate from direct non-canonical interaction with MED1 as well as from a distal allosteric  
36 effect.  
37  
38  
39  
40  
41  
42  
43  
44  
45

46 As MED1 is a classical NR coactivator, it is recognized by NRs similarly to other  
47 coregulators, e.g. SRCs, and their binding sites overlap. Interestingly, significant differences could  
48 be observed between the VDR-RXR complex with MED1 described here and the analogue  
49 complexes with the SRCs. In presence of 1,25D3 only RXR AF-2 within the full VDR-RXR complex  
50 was insensitive to the binding of SRC-1 RID, indicating that it is primarily associated to VDR AF-2  
51 (92). However, RXR and its ligand modulate the interaction and in the presence of both VDR and  
52 RXR agonists SRC-1 RID binding has been shown to stabilize VDR AF-2 as well as RXR H3 (227-273)  
53 and H10-H11 (433-451) (81). Differences in binding mode between SRCs and MED1 were  
54  
55  
56  
57  
58  
59  
60

1  
2 previously suggested for ER where a single mutation differently affects MED1 and SRC-2 RID  
3 interaction (93), or for PPAR-RXR where RXR ligand only induces SRCs but not MED1 binding to  
4 RXR (83). Such differences in the binding modes could serve as molecular determinants of how  
5 the NRs discriminate between coactivators and sequentially recruit them.  
6  
7

8  
9 This work contributes to a growing number of studies revealing the complexity of  
10 coactivator binding to NRs. Extended characterization of allosteric mechanism within large NR  
11 coregulator complexes should increase the potential of novel targets for drug design and  
12 discovery programs.  
13  
14  
15

### 16 17 18 **Contributions**

19 A.Y.B. and S.C. purified the proteins and performed biophysical and structural analyses. M.B., S.H.  
20 and S.C. performed the structural mass-spectrometry experiments and analyzed the data. B.K.  
21 performed the NMR analysis. N.R. designed and supervised the study. A.Y.B. and N.R. wrote the  
22 manuscript with contribution from all the authors. All authors have given approval to the final  
23 version of the paper.  
24  
25  
26  
27  
28

### 29 **Acknowledgements**

30 We thank the staff of BM29 at ESRF for assistance in using the beamline. We thank the IGBMC  
31 cell culture service, Isabelle Kolb-Cheynel and Nathalie Troffer-Charlier (IGBMC) for insect cell  
32 production, Pascal Eberling (IGBMC) for peptide synthesis, Pierre Poussin-Courmontagne  
33 (IGBMC) for assistance with SEC-MALLS, Camille Kostmann (IGBMC) for assistance with surface  
34 plasmon resonance, Catherine Birck (IGBMC) for help with analytical ultracentrifugation data  
35 collection, as well as Carole Peluso-Iltis (IGBMC) for excellent technical assistance.  
36  
37  
38  
39  
40  
41

### 42 **Funding**

43 This study was supported by grants from the Agence Nationale de la Recherche ANR-13-BSV8-  
44 0024-01 from ANR. The authors acknowledge the support and the use of resources of the French  
45 Infrastructure for Integrated Structural Biology (FRISBI ANR-10-INBS-05, Instruct-ERIC, and grant  
46 ANR-10-LABX-0030-INRT, a French State fund managed by the Agence Nationale de la Recherche  
47 under the program Investissements d'Avenir ANR-10-IDEX-0002-02) and the French Proteomic  
48 Infrastructure ProFI ANR-10-INBS-08-03. The authors thank GIS IBISA and Région Alsace for  
49 financial support in purchasing a Synapt G2SI HDMS instrument. MB was supported by a  
50 fellowship from the Région Alsace. AYB was supported by a FRM fellowship (FDT20140930978).  
51  
52  
53  
54  
55  
56  
57  
58  
59  
60

**Supporting Information.** Additional supplementary methods and figures can be found in SI appendix.

## References

1. Lonard, D.M., and O'Malley, B.W. (2012) Nuclear receptor coregulators: modulators of pathology and therapeutic targets. *Nat Rev Endocrinol.* **8**, 598-604.
2. Giudici, M., Goni, S., Fan, R., and Treuter, E. (2015) Nuclear Receptor Coregulators in Metabolism and Disease. In: Herzig S. (eds) *Metabolic Control. Handbook of Experimental Pharmacology*, vol 233. Springer.
3. Jeronimo, C., and Robert, F. (2017) The Mediator Complex: At the Nexus of RNA Polymerase II Transcription. *Trends Cell Biol.* **27**, 765-783.
4. Soutourina, J. (2018) Transcription regulation by the Mediator complex. *Nat Rev Mol Cell Biol.* **19**, 262-274.
5. Verger, A., Monté, D., and Villeret, V. (2019) Twenty years of Mediator complex structural studies. *Biochem Soc Trans.* **47**, 399-410.
6. Kelleher, R.J., Flanagan, P.M., and Kornberg, R.D. (1990) A novel mediator between activator proteins and the RNA polymerase II transcription apparatus. *Cell.* **61**, 1209-1215.
7. Flanagan, P.M., Kelleher, R.J., Sayre, M.H., Tschochner, H., and Kornberg, R.D. (1991) A mediator required for activation of RNA polymerase II transcription in vitro. *Nature.* **350**, 436-438.
8. Fondell, J.D., Ge, H., and Roeder, R.G. (1996) Ligand induction of a transcriptionally active thyroid hormone receptor coactivator complex. *Proc Natl Acad Sci U S A.* **93**, 8329-8333.
9. Rachez, C., Suldan, Z., Ward, J., Chang, C.P., Burakov, D., Erdjument-Bromage, H., Tempst, P., and Freedman, L.P. (1998) A novel protein complex that interacts with the vitamin D3 receptor in a ligand-dependent manner and enhances VDR transactivation in a cell-free system. *Genes Dev.* **12**, 1787-1800.
10. Näär, A.M., Beurang, P.A., Zhou, S., Abraham, S., Solomon, W., and Tjian, R. (1999) Composite co-activator ARC mediates chromatin-directed transcriptional activation. *Nature.* **398**, 828-832.
11. Jiang, Y.W., Veschambre, P., Erdjument-Bromage, H., Tempst, P., Conaway, J.W., Conaway, R.C., and Kornberg, R.D. (1998) Mammalian mediator of transcriptional regulation and its

- possible role as an end-point of signal transduction pathways. *Proc Natl Acad Sci U S A.* **95**, 8538-8543.
12. Boyer, T.G., Martin, M.E., Lees, E., Ricciardi, R.P., and Berk, A.J. (1999) Mammalian Srb/Mediator complex is targeted by adenovirus E1A protein. *Nature.* **399**,276-279.
13. Malik, S., Gu, W., Wu, W., Qin, J., and Roeder, R.G. (2000) The USA-derived transcriptional coactivator PC2 is a submodule of TRAP/SMCC and acts synergistically with other PCs. *Mol Cell.* **5**, 753-760.
14. Ryu, S., and Tjian, R. (1999) Purification of transcription cofactor complex CRSP. *Proc Natl Acad Sci U S A.* **96**, 7137-7142.
15. Yuan, C.X., Ito, M., Fondell, J.D., Fu, Z.Y., and Roeder, R.G. (1998) The TRAP220 component of a thyroid hormone receptor- associated protein (TRAP) coactivator complex interacts directly with nuclear receptors in a ligand-dependent fashion. *Proc Natl Acad Sci U S A.* **95**, 7939-7944.
16. Rachez, C., Lemon, B.D., Suldan, Z., Bromleigh, V., Gamble, M., Näär, A.M., Erdjument-Bromage, H., Tempst, P., and Freedman, L.P. (1999) Ligand-dependent transcription activation by nuclear receptors requires the DRIP complex. *Nature.* **398**, 824-828.
17. Zhu, Y., Qi, C., Jain, S., Rao, M.S., and Reddy, J.K. (1997) Isolation and characterization of PBP, a protein that interacts with peroxisome proliferator-activated receptor. *J Biol Chem.* **272**, 25500-25506.
18. Kang, Y.K., Guermah, M., Yuan, C.X., and Roeder, R.G. (2002). The TRAP/Mediator coactivator complex interacts directly with estrogen receptors alpha and beta through the TRAP220 subunit and directly enhances estrogen receptor function in vitro. *Proc Natl Acad Sci U S A.* **99**, 2642-2647.
19. Ge, K., Guermah, M., Yuan, C.X., Ito, M., Wallberg, A.E., Spiegelman, B.M., and Roeder, R.G. (2002) Transcription coactivator TRAP220 is required for PPAR gamma 2-stimulated adipogenesis. *Nature.* **417**, 563-567.
20. Hittelman, A.B., Burakov, D., Iñiguez-Lluhí, J.A., Freedman, L.P., and Garabedian, M.J. (1999) Differential regulation of glucocorticoid receptor transcriptional activation via AF-1-associated proteins. *EMBO J.* **18**, 5380-5388.
21. Malik, S., Wallberg, A.E., Kang, Y.K., and Roeder, R.G. (2002) TRAP/SMCC/mediator-dependent transcriptional activation from DNA and chromatin templates by orphan nuclear receptor hepatocyte nuclear factor 4. *Mol Cell Biol.* **22**, 5626-5637.

- 1  
2 22. Wang, Q., Sharma, D., Ren, Y., and Fondell, J.D. (2002) A coregulatory role for the TRAP-  
3 mediator complex in androgen receptor-mediated gene expression. *J Biol Chem.* **277**, 42852-  
4 42858.  
5  
6  
7 23. Kim, J.H., Yang, C.K., Heo, K., Roeder, R.G., An, W., and Stallcup, M.R. (2008) CCAR1, a key  
8 regulator of mediator complex recruitment to nuclear receptor transcription complexes. *Mol*  
9 *Cell.* **31**, 510-519.  
10  
11  
12 24. Chen, W., Yang, Q., and Roeder, R.G. (2009) Dynamic interactions and cooperative functions  
13 of PGC-1alpha and MED1 in TRalpha-mediated activation of the brown-fat-specific UCP-1 gene.  
14 *Mol Cell.* **35**, 755-768.  
15  
16  
17 25. Wallberg, A.E., Yamamura, S., Malik, S., Spiegelman, B.M., and Roeder, R.G. (2003)  
18 Coordination of p300-mediated chromatin remodeling and TRAP/mediator function through  
19 coactivator PGC-1alpha. *Mol Cell.* **12**, 1137-1149.  
20  
21  
22 26. Iida, S., Chen, W., Nakadai, T., Ohkuma, Y., and Roeder, R.G. (2015) PRDM16 enhances nuclear  
23 receptor-dependent transcription of the brown fat-specific Ucp1 gene through interactions with  
24 Mediator subunit MED1. *Genes Dev.* **29**, 308-321.  
25  
26  
27 27. Harms, M.J., Lim, H.W., Ho, Y., Shapira, S.N., Ishibashi, J., Rajakumari, S., Steger, D.J., Lazar,  
28 M.A., Won, K.J., and Seale, P. (2015) PRDM16 binds MED1 and controls chromatin architecture  
29 to determine a brown fat transcriptional program. *Genes Dev.* **29**, 298-307.  
30  
31  
32 28. Nolte, R.T., Wisely, G.B., Westin, S., Cobb, J.E., Lambert, M.H., Kurokawa, R., Rosenfeld, M.G.,  
33 Willson, T.M., Glass, C.K., and Milburn, M.V. (1998) Ligand binding and co-activator assembly of  
34 the peroxisome proliferator-activated receptor-gamma. *Nature.* **395**, 137-143.  
35  
36  
37 29. Shiau, A.K., Barstad, D., Loria, P.M., Cheng, L., Kushner, P.J., Agard, D.A., and Greene, G.L.  
38 (1998) The structural basis of estrogen receptor/coactivator recognition and the antagonism of  
39 this interaction by tamoxifen. *Cell.* **95**, 927-937.  
40  
41  
42 30. Darimont, B.D., Wagner, R.L., Apriletti, J.W., Stallcup, M.R., Kushner, P.J., Baxter, J.D.,  
43 Fletterick, R.J., and Yamamoto, K.R. (1998) Structure and specificity of nuclear  
44 receptor-coactivator interactions. *Genes Dev* **12**, 3343-3356.  
45  
46  
47 31. Burakov, D., Wong, C.W., Rachez, C., Cheskis, B.J., and Freedman, L.P. (2000) Functional  
48 interactions between the estrogen receptor and DRIP205, a subunit of the heteromeric DRIP  
49 coactivator complex. *J Biol Chem.* **275**, 20928-20934.  
50  
51  
52 32. Ren, Y., Behre, E., Ren, Z., Zhang, J., Wang, Q., and Fondell, J.D. (2000) Specific structural  
53 motifs determine TRAP220 interactions with nuclear hormone receptors. Specific structural  
54  
55  
56  
57  
58  
59  
60

- 1 motifs determine TRAP220 interactions with nuclear hormone receptors. *Mol Cell Biol.* **20**, 5433-  
2 5446.  
3  
4  
5  
6 33. Lai, F., Orom, U.A., Cesaroni, M., Beringer, M., Taatjes, D.J., Blobel, G.A., and Shiekhattar, R.  
7 (2013) Activating RNAs associate with Mediator to enhance chromatin architecture and  
8 transcription. *Nature.* **494**, 497-501.  
9  
10  
11 34. Hsieh, C.L., Fei, T., Chen, Y., Li, T., Gao, Y., Wang, X., Sun, T., Sweeney, C.J., Lee, G.S., Chen, S.,  
12 et al. (2014) Enhancer RNAs participate in androgen receptor-driven looping that selectively  
13 enhances gene activation. *Proc Natl Acad Sci U S A.* **111**, 7319-7324.  
14  
15  
16 35. Step, S.E., Lim, H.W., Marinis, J.M., Prokesch, A., Steger, D.J., You, S.H., Won, K.J., and Lazar,  
17 M.A. (2014) Anti-diabetic rosiglitazone remodels the adipocyte transcriptome by redistributing  
18 transcription to PPAR $\gamma$ -driven enhancers. *Genes Dev.* **28**, 1018-1028.  
19  
20  
21 36. Kagey, M.H., Newman, J.J., Bilodeau, S., Zhan, Y., Orlando, D.A., van Berkum, N.L., Ebmeier,  
22 C.C., Goossens, J., Rahl, P.B., Levine, S.S., et al. (2010) Mediator and cohesin connect gene  
23 expression and chromatin architecture. *Nature.* **467**, 430-435.  
24  
25  
26 37. Sanyal, A., Lajoie, B.R., Jain, G., and Dekker, J. (2012) The long-range interaction landscape of  
27 gene promoters. *Nature.* **489**, 109-113.  
28  
29  
30 38. Chen, W., and Roeder, R.G. (2011) Mediator-dependent nuclear receptor function. *Semin Cell*  
31 *Dev Biol.* **22**, 749-758.  
32  
33  
34 39. Meyer, M.B., and Pike, J.W. (2013) Corepressors (NCoR and SMRT) as well as coactivators are  
35 recruited to positively regulated 1 $\alpha$ ,25-dihydroxyvitamin D<sub>3</sub>-responsive genes. *J Steroid Biochem*  
36 *Mol Biol.* **136**, 120-124.  
37  
38  
39 40. Whyte, W.A., Orlando, D.A., Hnisz, D., Abraham, B.J., Lin, C.Y., Kagey, M.H., Rahl, P.B., Lee,  
40 T.I., and Young, R.A. (2013) Master transcription factors and mediator establish super-enhancers  
41 at key cell identity genes. *Cell.* **153**, 307-319.  
42  
43  
44 41. Lovén, J., Hoke, H.A., Lin, C.Y., Lau, A., Orlando, D.A., Vakoc, C.R., Bradner, J.E., Lee, T.I., and  
45 Young, R.A. (2013). Selective inhibition of tumor oncogenes by disruption of super-enhancers.  
46 *Cell.* **153**, 320-334.  
47  
48  
49 42. Sabari, B.R., Dall'Agnesse, A., Boija, A., Klein, I.A., Coffey, E.L., Shrinivas, K., Abraham, B.J.,  
50 Hannett, N.M., Zamudio, A.V., Manteiga, J.C., et al. (2018) Coactivator condensation at super-  
51 enhancers links phase separation and gene control. *Science.* **361**, 6400.  
52  
53  
54  
55  
56  
57  
58  
59  
60

- 1  
2 43. Chen, W., Zhang, X., Birsoy, K., and Roeder, R.G. (2010) A muscle-specific knockout implicates  
3 nuclear receptor coactivator MED1 in the regulation of glucose and energy metabolism. *Proc Natl*  
4 *Acad Sci U S A.* **107**, 10196-101201.  
5  
6  
7 44. Bai, L., Jia, Y., Viswakarma, N., Huang, J., Vluggens, A., Wolins, N.E., Jafari, N., Rao, M.S.,  
8 Borensztajn, J., Yang, G., et al. (2011) Transcription coactivator mediator subunit MED1 is  
9 required for the development of fatty liver in the mouse *Hepatology.* **53**, 1164-1174.  
10  
11  
12 45. Weber, H., and Garabedian, M.J. (2018) The mediator complex in genomic and non-genomic  
13 signaling in cancer. *Steroids.* **133**, 8-14.  
14  
15  
16 46. Osz, J., Brélivet, Y., Peluso-Iltis, C., Cura, V., Eiler, S., Ruff, M., Bourguet, W., Rochel, N., and  
17 Moras, D. (2012) Structural basis for a molecular allosteric control mechanism of cofactor binding  
18 to nuclear receptors. *Proc Natl Acad Sci U S A.* **109**, E588-594.  
19  
20  
21 47. Rochel, N., Ciesielski, F., Godet, J., Moman, E., Roessle, M., Peluso-Iltis, C., Moulin, M.,  
22 Haertlein, M., Callow, P., Mély, Y., et al. (2011) Common architecture of nuclear receptor  
23 heterodimers on DNA direct repeat elements with different spacings. *Nat Struct Mol Biol.* **18**,  
24 564-570.  
25  
26  
27 48. Pavlin, M.R., Brunzelle, J.S., and Fernandez, E.J. (2014) Agonist ligands mediate the  
28 transcriptional response of nuclear receptor heterodimers through distinct stoichiometric  
29 assemblies with coactivators. *J Biol Chem.* **289**, 24771-24778.  
30  
31  
32 49. Yi, P., Wang, Z., Feng, Q., Pintilie, G.D., Foulds, C.E., Lanz, R.B., Ludtke, S.J., Schmid, M.F., Chiu,  
33 W., and O'Malley, B.W. (2015) Structure of a biologically active estrogen receptor-coactivator  
34 complex on DNA. *Mol Cell.* **57**, 1047-1058.  
35  
36  
37 50. Yi, P., Wang, Z., Feng, Q., Chou, C.K., Pintilie, G.D., Shen, H., Foulds, C.E., Fan, G., Serysheva,  
38 I., Ludtke, S.J., et al. (2017) Structural and Functional Impacts of ER Coactivator Sequential  
39 Recruitment. *Mol Cell.* **67**, 733-743.  
40  
41  
42 51. Pernot, P., Theveneau, P., Giraud, T., Nogueira Fernandes, R., Nurizzo, D., Spruce, D., Surr, J.,  
43 McSweeney, S., Round, A., Felisaz, F., et al. (2010) New beamline dedicated to solution scattering  
44 from biological macromolecules at the ESRF. *Journal of Physics: Conference Series* **247**, 012009-  
45 1-012009-8.  
46  
47  
48 52. Konarev, P.V., Volkov, V.V., Sokolova, A.V., Koch, M.H.J. and Svergun, D.I. (2003) PRIMUS: a  
49 Windows PC-based system for small-angle scattering data analysis. *J. Appl. Cryst.* **36**, 1277-1282.  
50  
51  
52 53. Svergun, D.I. (1992) Determination of the regularization parameter in indirect-transform  
53 methods using perceptual criteria. *J. Appl. Cryst.* **25**, 495-503.  
54  
55  
56  
57  
58  
59  
60

- 1  
2 54. Petoukhov, M.V., and Svergun, D.I. (2005) Global rigid body modeling of macromolecular  
3 complexes against small-angle scattering data. *Biophys J.* **89**, 1237-1250.  
4  
5 55. Orlov, I., Rochel, N., Moras, D., and Klaholz, B.P. (2012) Structure of the full human RXR/VDR  
6 nuclear receptor heterodimer complex with its DR3 target DNA. *EMBO J.* **31**, 291-300.  
7  
8 56. Svergun, D.I., Barberato, C. and Koch, M.H.J. (1995) CRY SOL - a program to evaluate X-ray  
9 solution scattering of biological macromolecules from atomic coordinates. *J. Appl. Cryst.* **28**, 768-  
10 773.  
11  
12 57. Schuck, P., 2000. Size-distribution analysis of macromolecules by sedimentation velocity  
13 ultracentrifugation and lamm equation modeling. *Biophysical J.* **78**, 1606–1619.  
14  
15 58. Hourdel, V., Volant, S., O'Brien, D.P., Chenal, A., Chamot-Rooke, J., Dillies, M.A., and Brier S.  
16 (2016) MEMHDX: an interactive tool to expedite the statistical validation and visualization of  
17 large HDX-MS datasets. *Bioinformatics.* **32**, 3413-3419.  
18  
19 59. Perez-Riverol Y., Csordas A., Bai J., Bernal-Llinares M., Hewapathirana S., Kundu D.J., Inuganti  
20 A., Griss J., Mayer G., Eisenacher M., et al. (2019) The PRIDE database and related tools and  
21 resources in 2019: improving support for quantification data. *Nucleic Acids Res.* **47**,442-D450.  
22  
23 60. Götze, M., Pettelkau, J., Fritzsche, R., Ihling, C., Schäfer, M., and Sinz, A. (2015) Automated  
24 assignment of MS/MS cleavable cross-links in protein 3D-structure analysis. *J. Am. Soc. Mass.*  
25 *Spec.* **26**, 83-97.  
26  
27 61. Teichert, A., Arnold, L.A., Otieno, S., Oda, Y., Augustinaite, I., Geistlinger, T.R., Kriwacki, R.W.,  
28 Guy, R.K., and Bikle, D.D. (2009) Quantification of the vitamin D receptor-coregulator interaction.  
29 *Biochemistry.* **48**, 1454-1461.  
30  
31 62. Ge, K., Cho, Y.W., Guo, H., Hong, T.B., Guermah, M., Ito, M., Yu, H., Kalkum, M., and Roeder,  
32 R.G. (2008) Alternative mechanisms by which mediator subunit MED1/TRAP220 regulates  
33 peroxisome proliferator-activated receptor gamma-stimulated adipogenesis and target gene  
34 expression. *Mol Cell Biol.* **28**, 1081-1091.  
35  
36 63. Kahlen, J.P., and Carlberg, C. (1996) Functional characterization of a 1,25-dihydroxyvitamin  
37 D3 receptor binding site found in the rat atrial natriuretic factor promoter. *Biochem Biophys Res*  
38 *Commun.* **218**, 882-886.  
39  
40 64 Svergun, D.I. (1999) Restoring low resolution structure of biological macromolecules from  
41 solution scattering using simulated annealing. *Biophys J.* **76**, 2879-2886.  
42  
43 65. Rochel, N., Wurtz, J.M., Mitschler, A., Klaholz, B., and Moras, D. (2000) The crystal structure  
44 of the nuclear receptor for vitamin D bound to its natural ligand. *Mol Cell.* **5**, 173-179.  
45  
46  
47  
48  
49  
50  
51  
52  
53  
54  
55  
56  
57  
58  
59  
60

- 1  
2 66. Egea, P.F., Mitschler, A., Rochel, N., Ruff, M., Chambon, P., and Moras, D. (2000) Crystal  
3 structure of the human RXRalpha ligand-binding domain bound to its natural ligand: 9-cis retinoic  
4 acid. *EMBO J.* **19**, 2592-2601.  
5  
6  
7 67. Shaffer, P.L., and Gewirth, D.T. (2002) Structural basis of VDR-DNA interactions on direct  
8 repeat response elements. *EMBO J.* **21**, 2242-2252.  
9  
10  
11 68. Rochel, N., Tocchini-Valentini, G., Egea, P.F., Juntunen, K., Garnier, J.M., Vihko, P., and Moras,  
12 D. (2001) Functional and structural characterization of the insertion region in the ligand binding  
13 domain of the vitamin D nuclear receptor. *Eur J Biochem.* **268**, 971-979.  
14  
15  
16 69. Belorusova, A.Y., Chalhoub, S., Rovito, D., and Rochel N. (2020) Structural analysis of VDR  
17 complex with ZK168281 antagonist. *J Med Chem* **2020**, doi: 10.1021/acs.jmedchem.0c00656..  
18  
19  
20 70. Rachez, C., Gamble, M., Chang, C.P., Atkins, G.B., Lazar, M.A., and Freedman, L.P. (2000) The  
21 DRIP complex and SRC-1/p160 coactivators share similar nuclear receptor binding determinants  
22 but constitute functionally distinct complexes. *Mol Cell Biol.* **20**, 2718-2726.  
23  
24  
25 71. Gampe, R.T. Jr, Montana, V.G., Lambert, M.H., Miller, A.B., Bledsoe, R.K., Milburn, M.V.,  
26 Kliewer, S.A., Willson, T.M., and Xu, HHE.. (2000) Asymmetry in the PPARgamma/RXRalpha  
27 crystal structure reveals the molecular basis of heterodimerization among nuclear receptors. *Mol*  
28 *Cell* **5**,545-555.  
29  
30  
31 72. Pogenberg, V., Guichou, J.F., Vivat-Hannah, V., Kammerer, S., Pérez, E., Germain, P., de Lera,  
32 A.R., Gronemeyer, H., Royer, C.A., and Bourguet, W. (2005) Characterization of the interaction  
33 between retinoic acid receptor/retinoid X receptor (RAR/RXR) heterodimers and transcriptional  
34 coactivators through structural and fluorescence anisotropy studies. *J Biol Chem.* **280**, 1625-  
35 1633.  
36  
37  
38 73. Keppel, T.R., Howard, B.A., and Weis, D.D. (2011) Mapping Unstructured Regions and  
39 Synergistic Folding in Intrinsically Disordered Proteins with Amide H/D Exchange Mass  
40 Spectrometry. *Biochemistry.* **50**, 8722–8732.  
41  
42  
43 74. Vanhooke, J.L., Benning, M.M., Bauer, C.B., Pike, J.W., and DeLuca, H.F. (2004) Molecular  
44 structure of the rat vitamin D receptor ligand binding domain complexed with 2-carbon-  
45 substituted vitamin D3 hormone analogues and a LXXLL-containing coactivator peptide.  
46 *Biochemistry.* **43**, 4101-4110.  
47  
48  
49 75. Ciesielski, F., Rochel, N., Mitschler, A., Kouzmenko, A., and Moras, D. (2004) Structural  
50 investigation of the ligand binding domain of the zebrafish VDR in complexes with  
51  
52  
53  
54  
55  
56  
57  
58  
59  
60

- 1  
2 1alpha,25(OH)2D3 and Gemini: purification, crystallization and preliminary X-ray diffraction  
3  
4 analysis. *J Steroid Biochem Mol Biol.* **89-90**, 55-59.
- 5  
6 76. Stafslie, D.K., Vedvik, K.L., De Rosier, T., and Ozers, M.S. (2007) Analysis of ligand-dependent  
7  
8 recruitment of coactivator peptides to RXRbeta in a time-resolved fluorescence resonance  
9  
10 energy transfer assay. *Mol Cell Endocrinol.* **264**, 82-89.
- 11  
12 77. Müller, M.Q., Dreiocker, F., Ihling, C.H., Schäfer, M., and Sinz, A. (2010) Cleavable Cross-linker  
13  
14 for Protein Structure Analysis: Reliable Identification of Cross-linking Products by Tandem MS.  
15  
16 *Anal. Chem.* **82**, 6958-6968.
- 17  
18 78. Arlt, C., Goetze, M., Ihling, C.H., Hage, C., Schaefer, M., and Sinz A. (2016) An Integrated  
19  
20 Workflow for Structural Proteomics Studies based on Cross-linking/Mass Spectrometry with an  
21  
22 MS/MS Cleavable Cross-linker. *Anal. Chem.* **88**, 7930-7937.
- 23  
24 79. Merkle, E.D., Rysavy, S., Kahraman, A., Hafen, R.P., Daggett, V., and Adkins, J.N. (2014)  
25  
26 Distance restraints from crosslinking mass spectrometry: Mining a molecular dynamics  
27  
28 simulation database to evaluate lysine-lysine distances. *Protein Sci.* **23**, 747-759.
- 29  
30 80. Weikum, E.R., Liu, X., and Ortlund, E.A. (2018) The nuclear receptor superfamily: A structural  
31  
32 perspective. *Protein Sci.* **27**, 1876-1892.
- 33  
34 81. Zhang, J., Chalmers, M.J., Stayrook, K.R., Burris, L.L., Wang, Y., Busby, S.A., Pascal, B.D., Garcia-  
35  
36 Ordonez, R.D., Bruning, J.B., Istrate, M.A., et al. (2011) DNA binding alters coactivator interaction  
37  
38 surfaces of the intact VDR-RXR complex. *Nat Struct Mol Biol.* **18**, 556-563.
- 39  
40 82. Oda, Y., Hu, L., Bul, V., Elalieh, H., Reddy, J.K., and Bikle, D.D. (2012) Coactivator MED1  
41  
42 ablation in keratinocytes results in hair-cycling defects and epidermal alterations. *J Invest*  
43  
44 *Dermatol.* **132**, 1075-1083.
- 45  
46 83. Yang, W., Rachez, C., and Freedman, L.P. (2000) Discrete roles for peroxisome proliferator-  
47  
48 activated receptor gamma and retinoid X receptor in recruiting nuclear receptor coactivators.  
49  
50 *Mol Cell Biol.* **20**, 8008-8017.
- 51  
52 84. Malik, S., Guermah, M., Yuan, C.X., Wu, W., Yamamura, S., and Roeder, R.G. (2004) Structural  
53  
54 and functional organization of TRAP220, the TRAP/mediator subunit that is targeted by nuclear  
55  
56 receptors. *Mol Cell Biol.* **24**, 8244-8254.
- 57  
58 85. Jiménez-Lara, A.M., and Aranda, A. (1999) Lysine 246 of the vitamin D receptor is crucial for  
59  
60 ligand-dependent interaction with coactivators and transcriptional activity. *J Biol Chem.* **274**,  
13503-13510.

- 1  
2 86. de Vera, I.M.S., Zheng, J., Novick, S., Shang, J., Hughes, T.S., Brust, R., Munoz-Tello, P.,  
3 Gardner, W.J. Jr, Marciano, D.P., Kong, X., et al. (2017) Synergistic Regulation of  
4 Coregulator/Nuclear Receptor Interaction by Ligand and DNA. *Structure*. **25**, 1506-1518.  
5  
6 87. Jin, F., Claessens, F., and Fondell, J.D. (2012) Regulation of androgen receptor-dependent  
7 transcription by coactivator MED1 is mediated through a newly discovered noncanonical binding  
8 motif. *J Biol Chem*. **287**, 858-870.  
9  
10 88. Krasowski, M.D., Ai, N., Hagey, L.R., Kollitz, E.M., Kullman, S.W., Reschly, E.J., and Ekins, S.  
11 (2011) The evolution of farnesoid X, vitamin D, and pregnane X receptors: insights from the  
12 green-spotted pufferfish (*Tetraodon nigriviridis*) and other non-mammalian species. *BMC*  
13 *Biochem*. **12**, 5.  
14  
15 89. Zenata, O., and Vrzal, R. (2017) Fine tuning of vitamin D receptor (VDR) activity by post-  
16 transcriptional and post-translational modifications. *Oncotarget*. **8**, 35390-35402.  
17  
18 90. Barletta, F., Freedman, L.P., and Christakos, S. (2002) Enhancement of VDR-mediated  
19 transcription by phosphorylation: correlation with increased interaction between the VDR and  
20 DRIP205, a subunit of the VDR-interacting protein coactivator complex. *Mol Endocrinol*. **16**, 301-  
21 314.  
22  
23 91. Arriagada, G., Paredes, R., Olate, J., van Wijnen, A., Lian, J.B., Stein, G.S., Stein, J.L., Onate, S.,  
24 and Montecino, M. (2007) Phosphorylation at serine 208 of the 1 $\alpha$ ,25-dihydroxy Vitamin D3  
25 receptor modulates the interaction with transcriptional coactivators. *J Steroid Biochem Mol Biol*.  
26 **103**, 425-429.  
27  
28 92. Zheng, J., Chang, M.R., Stites, R.E., Wang, Y., Bruning, J.B., Pascal, B.D., Novick, S.J., Garcia-  
29 Ordonez, R.D., Stayrook, K.R., Chalmers, M.J., et al. (2017) HDX reveals the conformational  
30 dynamics of DNA sequence specific VDR co-activator interactions. *Nat Commun*. **8**, 923.  
31  
32 93. Acevedo, M.L., Lee, K.C., Stender, J.D., Katzenellenbogen, B.S., and Kraus, W.L. (2004)  
33 Selective recognition of distinct classes of coactivators by a ligand-inducible activation domain.  
34 *Mol Cell*. **13**, 725-738.  
35  
36  
37  
38  
39  
40  
41  
42  
43  
44  
45  
46  
47  
48  
49  
50  
51  
52

### Figure Legends

53  
54 **Figure 1. MED1 forms a complex with VDR-RXR-DNA. (a)** Size-exclusion chromatography-  
55 coupled multi-angle laser light scattering (SEC-MALLS) of MED1, VDR-RXR-DNA and VDR-RXR-  
56 DNA-MED1 complexes showing the elution profile on a SEC S200 10/300 with the direct molar  
57  
58  
59  
60

1  
2 mass measurement of each elution peak. **(b)** Analytical ultracentrifugation:  $c(s)$  distributions.  
3  
4 Ratio MED1:VDR-RXR-DNA is indicated and is used for the color representation of the  
5  
6 distributions. Left side of the graph corresponds to the top, and right side – to the bottom of the  
7  
8 sample cell, which correlates with the direction of migration. **(c)** Analysis of the interactions of  
9  
10 VDR-RXR wild type and VDR-RXR $\Delta$ H12, VDR-RXR AF-2Mutant and VDR $\Delta$ 12-RXR mutants with  
11  
12 MED1 (50-660) in the presence of 1,25D3 and 9cis RA by surface plasmon resonance and  
13  
14 calculated  $K_D$ .

15 **Figure 2. Solution structure of MED1 complex with VDR-RXR-DNA.** **(a)** Averaged SEC-SAXS data  
16  
17 for VDR-RXR-DNA (blue) and VDR-RXR-DNA-MED1 (green) complexes. **(b)** Corresponding  $p(r)$   
18  
19 profiles calculated from the SAXS data. **(c)** Representative *ab initio* molecular envelopes for VDR-  
20  
21 RXR-DNA-MED1 complex (green mesh) with superimposed *ab initio* molecular envelope of VDR-  
22  
23 RXR-DNA (blue mesh). **(d)** SAXS-based ensemble models (4 conformations) of the VDR-RXR-DNA  
24  
25 complex. **(e)** Best SAXS model of VDR-RXR-DNA fitted into the SAXS envelope of VDR-RXR-DNA-  
26  
27 MED1. **(f)**  $^1\text{H}$ - $^{15}\text{N}$  HSQC spectra of the VDR-RXR-DNA complex lacking the VDR LBD insertion  
28  
29 before (blue) and after addition of stoichiometric amount of MED1 (red), **(g)**  $^1\text{H}$ - $^{15}\text{N}$  HSQC spectra  
30  
31 of the VDR-RXR-DNA complex harboring the full-length VDR before (blue) and after addition of  
32  
33 stoichiometric amount of MED1 (red). The red stars indicate correlation peaks whose intensities  
34  
35 are affected by the addition of MED1.

36 **Figure 3. HDX-MS analysis of the VDR-RXR-DNA interaction with MED1.** **(a)** Relative fractional  
37  
38 uptake (RFU) differences between VDR-RXR-DNA and VDR-RXR-DNA-MED1 NR Box 2 complexes  
39  
40 mapped on the representative SAXS model of the VDR-RXR-rDNA after 0.5 minutes of  
41  
42 deuteration. **(b)** Relative fractional uptake (RFU) differences between VDR-RXR-DNA and VDR-  
43  
44 RXR-DNA-MED1 (50-660) complexes mapped on the representative SAXS model of the VDR-RXR-  
45  
46 DNA after 0.5 minutes of deuteration. **(c)** Deuterium uptake of the peptides 224-230 (H3), 385-  
47  
48 389 (H10) and 413-419 (H11-12) from VDR perturbed upon MED1 (50-660) binding plotted as a  
49  
50 function of deuteration time. **(d)** Deuterium uptake of the peptides 271-278 (H3), 326-330 ( $\beta$ )  
51  
52 and 450-454 (H12) from RXR perturbed upon MED1 (50-660) binding plotted as a function of  
53  
54 deuteration time. **(e)** Deuterium uptake of selected MED1 peptides perturbed upon binding to  
55  
56 VDR-RXR-DNA: 243-255 from the structured N-terminal part, 595-604 comprising Leu604 of the  
57  
58 NR Box 1 and 636-645 comprising Leu645 from the NR Box 2.

59 **Figure 4. Crosslinked sites observed for the VDR-RXR-DNA-MED1(50-660) complex.** **(a)**  
60  
61 Identified VDR-RXR-MED1 (50-660) crosslinks representation. Red: NR boxes 1 and 2 of MED1;

1  
2 purple: LBD region; grey: hinge region; pink: DBD region for each nuclear receptor, VDR and RXR.  
3  
4 Blue lines represent inter-protein crosslinks and purple curved lines intra-protein crosslinks. **(b)**  
5  
6 Representation of Lys321 of RXR, identifies as crosslinked to Thr236 of MED1, within the VDR-  
7  
8 RXR LBD heterodimer.

9  
10 **Figure 5. Schematic representation of MED1 binding to liganded VDR-RXR-DNA complex.** As we  
11 show in this study, while complex formation is primarily driven by a strong ligand-dependent  
12 MED1 NR2 binding to the VDR AF-2 (1), other MED1 regions including NR1 (2) and the structured  
13 N-terminal domain (3) are involved in the interaction, as well as alternative sites of the receptors  
14 including VDR insertion domain (4) and RXR (5).  
15  
16  
17  
18  
19  
20  
21  
22  
23  
24  
25  
26  
27  
28  
29  
30  
31  
32  
33  
34  
35  
36  
37  
38  
39  
40  
41  
42  
43  
44  
45  
46  
47  
48  
49  
50  
51  
52  
53  
54  
55  
56  
57  
58  
59  
60

**Table 1. SAXS parameters.**  $R_g$  and  $D_{max}$  as determined from Guinier plot or  $p(r)$  distribution.

Sample	$R_g$ , Å (from Guinier plot)	$R_g$ , Å (from GNOM)	$D_{max}$ , Å (from GNOM)
VDR-RXR-DNA-MED1	$63.8 \pm 2.3$	$63.6 \pm 0.13$	202
VDR-RXR-DNA	$42.8 \pm 0.14$	$43.3 \pm 0.1$	135
MED1	$41.5 \pm 0.27$	$41.6 \pm 0.12$	140

Figure 1

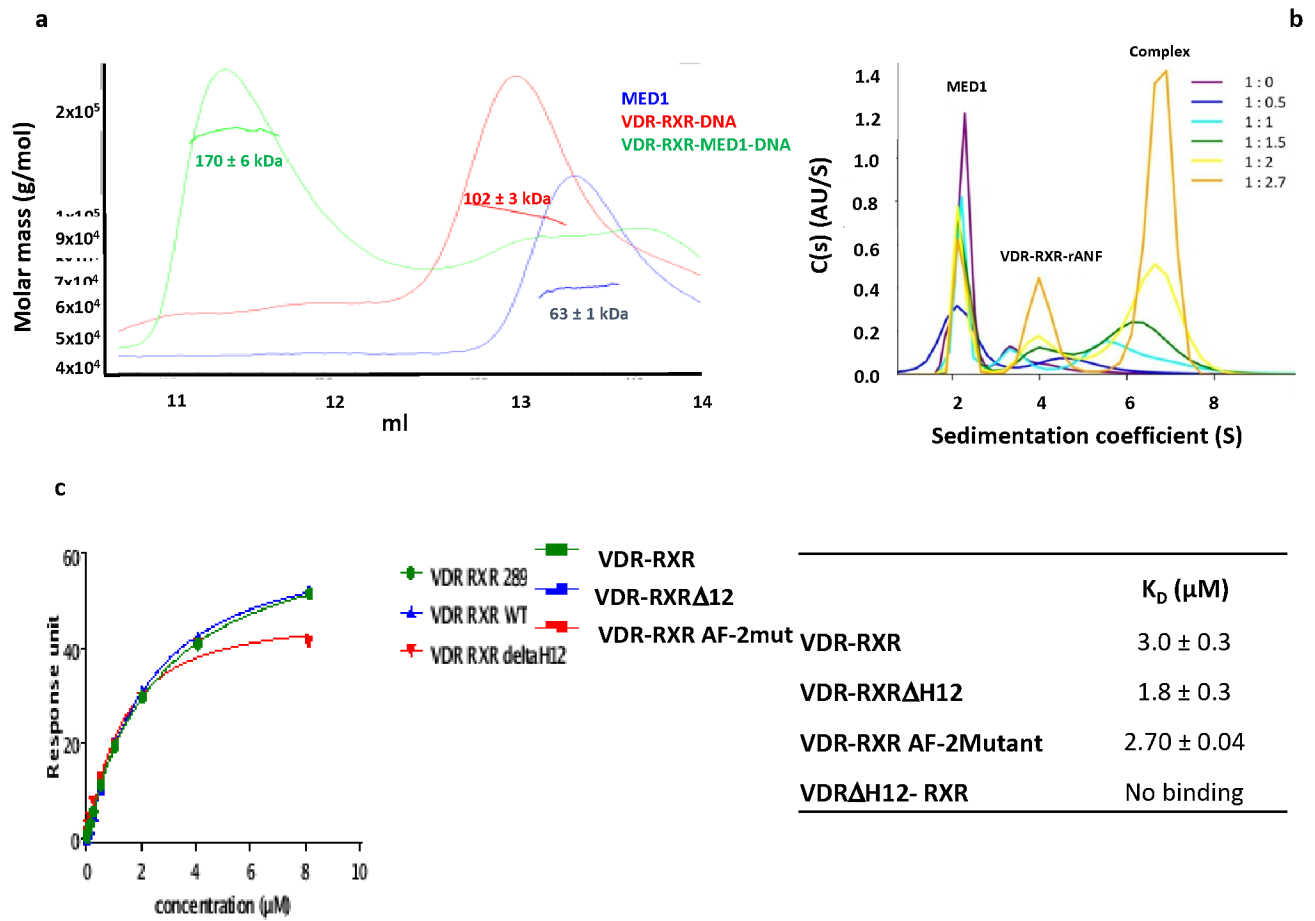


Figure 2

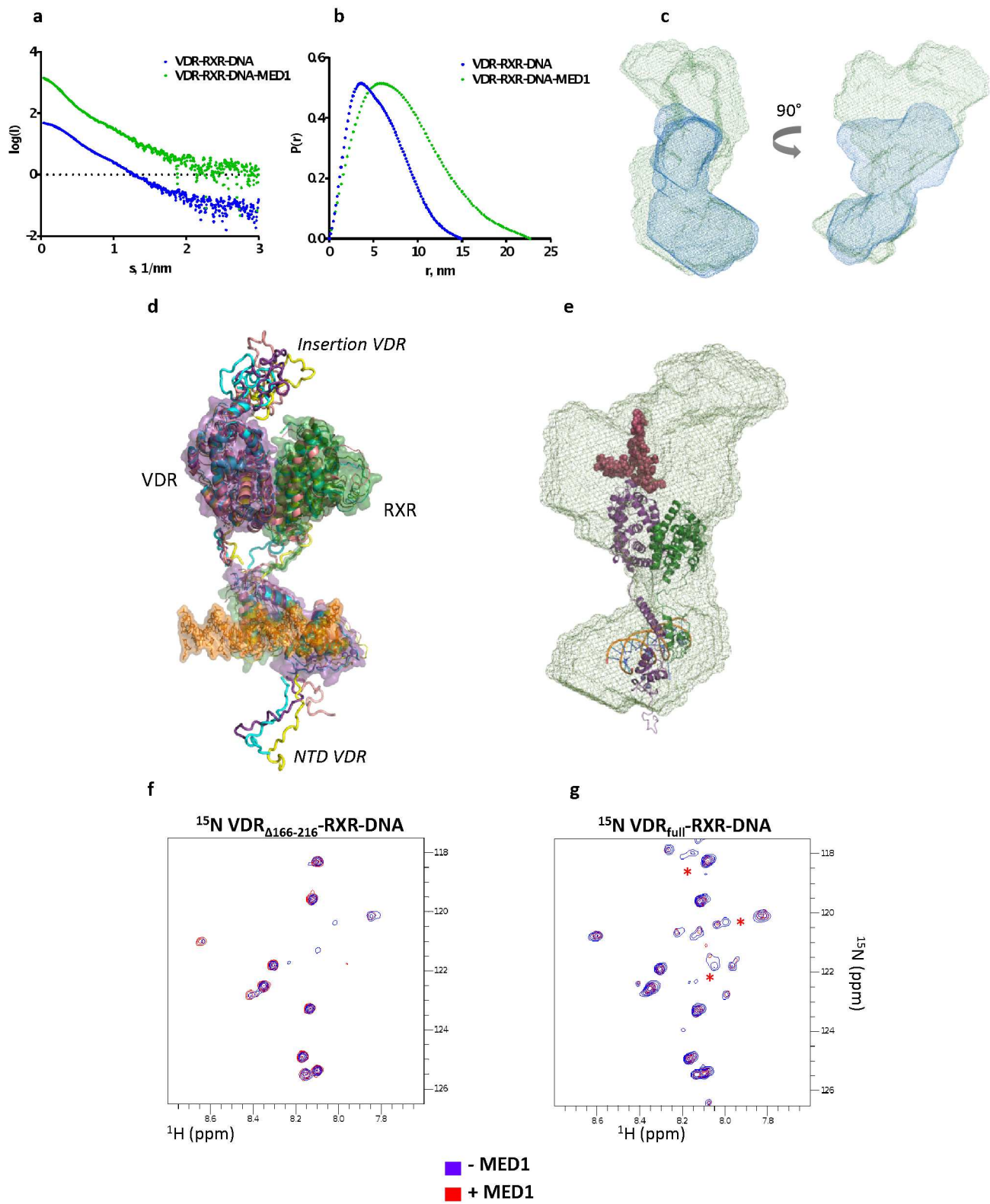


Figure 3

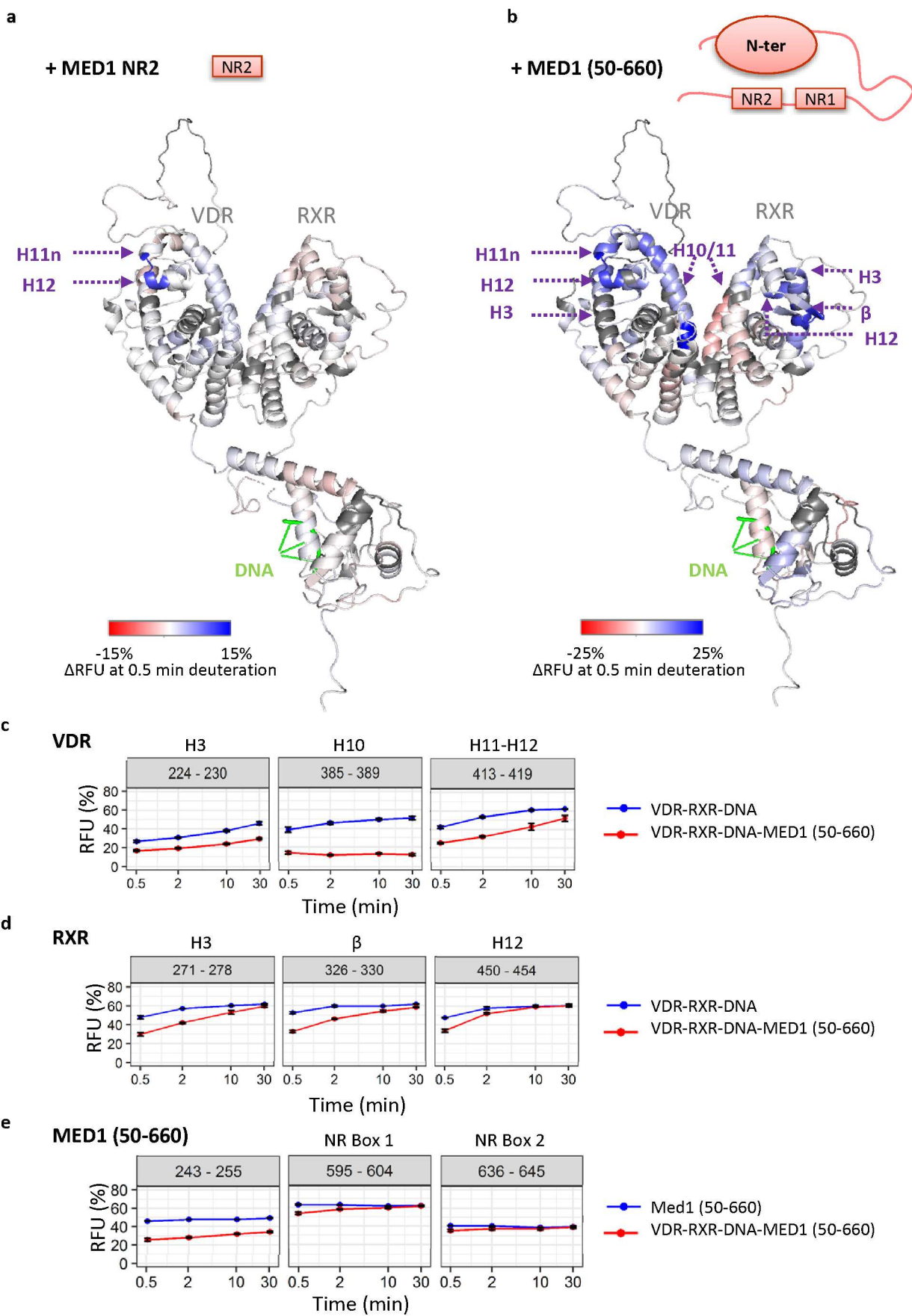
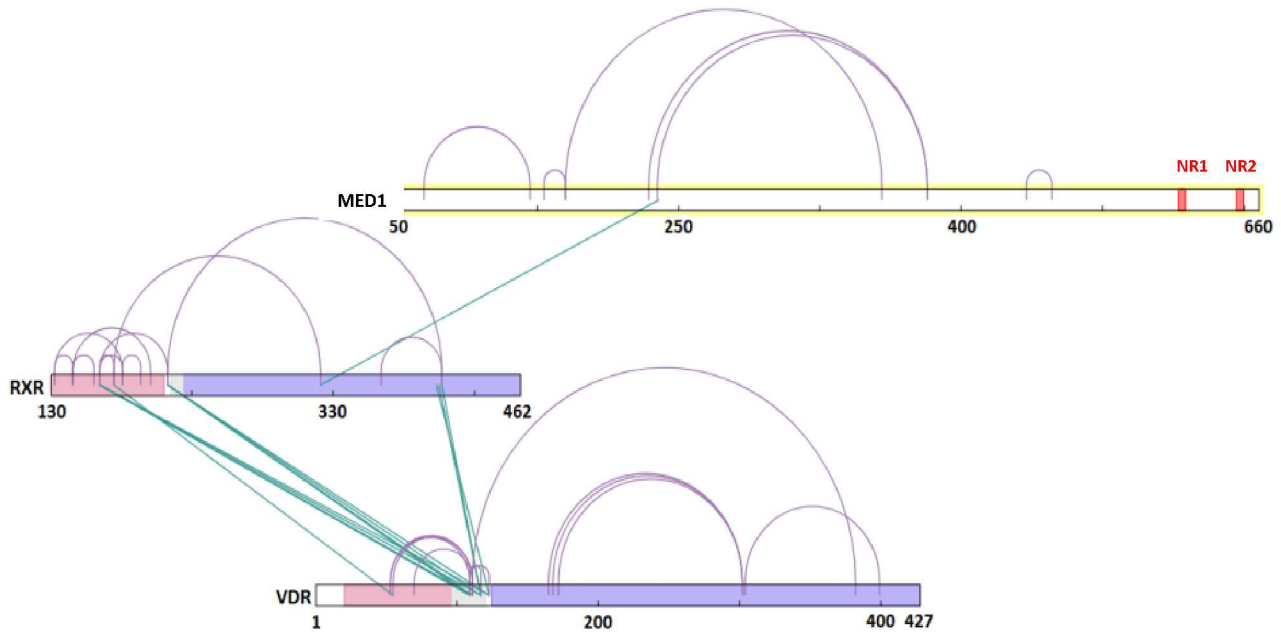
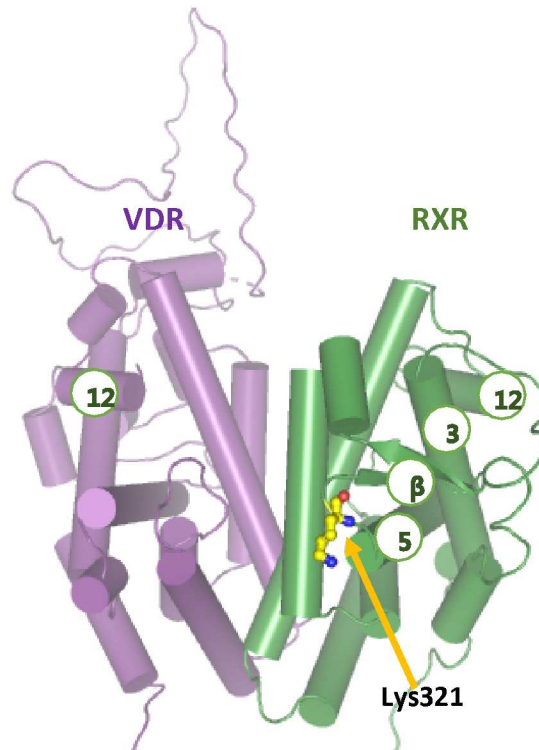


Figure 4

a

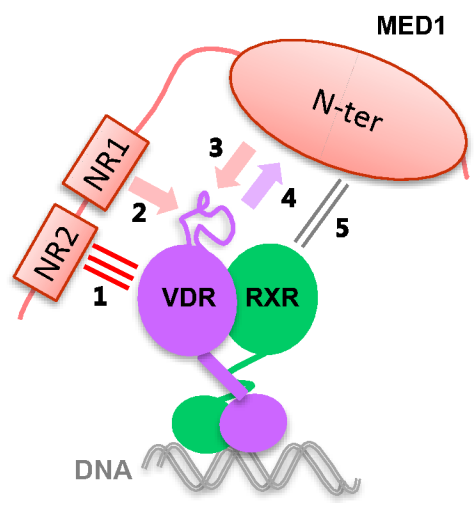


b



1  
2  
3  
4  
5  
6  
7  
8  
9  
10  
11  
12  
13  
14  
15  
16  
17  
18  
19  
20  
21  
22  
23  
24  
25  
26  
27  
28  
29  
30  
31  
32  
33  
34  
35  
36  
37  
38  
39  
40  
41  
42  
43  
44  
45  
46  
47  
48  
49  
50  
51  
52  
53  
54  
55  
56  
57  
58  
59  
60

Figure 5



## Supplementary data

### Molecular determinants of MED1 interaction with the DNA bound VDR-RXR heterodimer

Anna Y. Belorusova<sup>1-4,#</sup> ✉, Maxime Bourguet<sup>5,#</sup>, Steve Hessmann<sup>5</sup>, Sandra Chalhoub<sup>1-4</sup>, Bruno Kieffer<sup>1-4</sup>, Sarah Cianférani<sup>5</sup>, Natacha Rochel<sup>1-4</sup> ✉

<sup>1</sup>Institut de Génétique et de Biologie Moléculaire et Cellulaire (IGBMC), Illkirch, France.

<sup>2</sup>Centre National de la Recherche Scientifique UMR7104, Illkirch, France.

<sup>3</sup>Institut National de la Santé et de la Recherche Médicale U1258, Illkirch, France.

<sup>4</sup>Université de Strasbourg, Illkirch, France.

<sup>5</sup>Laboratoire de Spectrométrie de Masse BioOrganique, Université de Strasbourg, CNRS UMR 7178, IPHC, Strasbourg, France

#Co-first authors

✉ Correspondence to [Anna Y. Belorusova \(anna.y.belorusova@gmail.com\)](mailto:anna.y.belorusova@gmail.com) or [Natacha Rochel \(rochel@igbmc.fr\)](mailto:rochel@igbmc.fr)

### Supplementary Methods

**Isothermal titration calorimetry.** Measurements were performed at 15°C on a MicroCal ITC200 (MicroCal). Oligonucleotides and purified VDR-RXR were dialyzed extensively against the buffer containing 20 mM HEPES pH 7.5, 100 mM NaCl, 5% Glycerol, 1 mM TCEP overnight. Direct titration experiments were performed as follows: 2 µL aliquots of DR3 at 75–150 µM were injected into a 7.5 – 15 µM VDR-RXR solution in a 200 µL sample cell. The duration of each injection was 4 s with a delay between injections of 120 s. ITC titration curves were analyzed using the software Origin 7.0 (OriginLab). Standard free energies of binding and entropic contributions were obtained, respectively, as  $\Delta G = -RT\ln(K_a)$  and  $T\Delta S = \Delta H - \Delta G$ , where the association constant  $K_a$  and enthalpy change  $\Delta H$  values were derived from ITC curve fitting.

### Reporter gene assay

HEK293 EBNA cells were plated into 24-well plates at 105 cells per well and grown overnight in Dulbecco's modified Eagle's medium (DMEM) supplemented with 10% charcoal- treated

1  
2  
3 fetal bovine serum (FCS) and 40  $\mu\text{g}/\text{mL}$  gentamycin. At 80% confluence cells were transfected  
4 with 1  $\mu\text{g}$  of pDNA per well using jetPEI (Polyplus transfection). Transfection was performed  
5 according to the manufacturer's instructions. The transfection mix consisted of the cells were  
6 transfected with 150ng of the expression plasmid pSG5-hVDR (1-427), 150 ng of the pSG5-  
7 hRXR $\alpha$  (1-462), 150 ng of the reporter plasmid containing the DR3-type *rANF1* vitamin D  
8 response element fused to the tk promoter, 3ng of the pRL plasmid (Promega) containing the  
9 Renilla luciferase gene (transfection and cell viability control), and 497 ng of the carrier  
10 plasmid pBlueScript (Stratagene). Eight hours post transfection, 1,25D3 or vehicle (ethanol)  
11 were added. Cells were harvested after eighteen hours of incubation with the ligand. The  
12 amounts of reporter gene product (firefly luciferase) and constitutively expressed Renilla  
13 luciferase produced in the cells were measured using Dual-Luciferase<sup>®</sup> Reporter Assay System  
14 (Promega) on a luminometer plate reader LB96P (Berthold Technologies). Luminescence of  
15 firefly luciferase values was normalized to the Renilla luciferase activity. Luciferase activities  
16 were expressed as relative light units (RLU) intensity. Assays were performed in triplicate for  
17 at least two independent experiments. For every triplicate, the mean and the standard error  
18 of the mean were calculated.  
19  
20  
21  
22  
23  
24  
25  
26  
27  
28  
29  
30  
31  
32  
33  
34

### 35 **Supplementary Figures Legend**

36 **Supplementary Figure 1. (a)** Structural organization of hMED1. **(b)** Disorder prediction for  
37 MED1 obtained by RONN (<http://www.strubi.ox.ac.uk/RONN>).  
38

39 **Supplementary Figure 2. VDR-RXR-DNA-MED1 complex. (a)** ITC binding isotherm (upper  
40 panel) and fit to the binding curve (lower panel) for *rANF1* DR3 binding to the VDR-RXR. **(b)**  
41 Transactivation assay in HEK293 EBNA cells co-transfected with pDNAs encoding full-length  
42 VDR and luciferase cloned with two copies of the *rANF1* VDRE. Luciferase activity was  
43 measured after 24 hours of the cell treatment with increasing amounts of 1,25D3. **(c)** Gel  
44 retardation in TBE. 6% acrylamide gel stained with Coomassie Blue. **(d)** Overlay of gel filtration  
45 chromatograms for VDR-RXR-DNA, MED1 and their mix, and **(e)** analysis of gel filtration  
46 fractions by a 10% SDS-PAGE gel. Fractions of interest are framed.  
47  
48  
49  
50  
51  
52  
53  
54

55 **Supplementary Figure 3. Sedimentation profiles of the MED1 binding reaction.** The  
56 MED1:VDR-RXR-DNA ratio is indicated above each box. Upper panels: raw sedimentation data  
57  
58  
59  
60

1  
2  
3 (dots) and fitted  $c(s)$  distributions. Lower panels: residuals of the  $c(s)$  fit. Early  
4 data/fits/residuals are colored violet, and later data are colored according to the rainbow.

5  
6 **Supplementary Figure 4. On-line SAXS coupled with SEC.** Gel filtration was performed on the  
7 Superdex S200 Increase column (GE Healthcare). (a) Elution profiles. (b) Plots of total  
8 scattering (upper panel) and radius of gyration (lower panel) vs. frame.

9  
10 **Supplementary Figure 5. SAXS analysis of MED1 (50-660).** (a) SAXS profile after an on-line GF  
11 separation together with the corresponding fit of the theoretical data for the refined model.  
12 (b)  $p(r)$  profile calculated from the SAXS data. (c) Kratky plot.

13  
14 **Supplementary Figure 6.** Relative fractional uptakes of VDR (a) and RXR (b) represented for  
15 VDR-RXR-DNA and VDR-RXR-DNA-MED1 NR Box 2 states at all deuteration times (0.5, 2, 10  
16 and 30 minutes). Red framed peptides correspond to highly flexible regions of these proteins,  
17 presenting fast exchange rates. Some of RFU plots of these regions are represented.

18  
19 **Supplementary Figure 7.** Relative fractional uptake difference plots represented for VDR (a)  
20 and RXR (b) profiles displaying change in HDX upon binding of MED1 NR Box 2 peptide. RFU  
21 differences are depicted for 0.5, 2, 10 and 30 minutes of deuteration. Framed peptides  
22 represent the most impacted regions of VDR upon NR2 motif binding presenting a statistical  
23 significance ( $p < 0.01$ , Wald Test, MEMHDX software) for the magnitude of the difference.  
24 Among them, blue highlighted peptides present RFU differences above 5% while grey  
25 highlighted peptides present RFU differences below 5%.

26  
27 **Supplementary Figure 8. Gel filtration profiles.** (a) Overlay of gel filtrations chromatograms  
28 of VDR-RXR-DNA-MED1 and VDR $\Delta$ H12-RXR-DNA-MED1 mix. (b) Overlay of gel filtrations  
29 chromatograms of VDR-RXR-DNA-MED1 mix in presence of 1,25D3 and 9cisRA, or ZK168281  
30 alone or ZK168281 and 9cis RA.

31  
32 **Supplementary Figure 9.** (a) Relative fractional uptake differences plots of MED1 (50-660)  
33 measured after 0.5, 2, 10 and 30 minutes of deuteration. (b) Disorder prediction for MED1. (c)  
34 Secondary structure prediction of MED1 (50-660) where  $\alpha$ -helices are indicated in red,  $\beta$ -  
35 strands in purple and random coil in green.

36  
37 **Supplementary Figure 10.** Relative fractional uptake difference plots of VDR (a) and RXR (b)  
38 in VDR-RXR-DNA and VDR-RXR-DNA-MED1 (50-660) states measured after 0.5, 2, 10 and 30  
39 minutes of deuteration. Framed peptides represent the most impacted regions of VDR and  
40 RXR upon MED1 (50-660) binding presenting a statistical significance ( $p < 0.01$ , Wald Test,  
41 MEMHDX software) for the magnitude of the difference. Among them, blue highlighted  
42  
43  
44  
45  
46  
47  
48  
49  
50  
51  
52  
53  
54  
55  
56  
57  
58  
59  
60

1  
2  
3 peptides present RFU differences above 5% while grey highlighted peptides present RFU  
4 differences below 5%.

5  
6 **Supplementary Figure 11.** HDX-MS characterization of MED1 (50-660). **(a)** Heat map  
7 representation of MED1 (50-660) where RFU differences between MED1 (50-660) and VDR-  
8 RXR-DNA-MED1 (50-660) complex are depicted for 0.5, 2, 10 and 30 minutes deuteration  
9 times with a color scheme representing RFU differences (-/+ 15% difference range). **(b)**  
10 Relative fractional uptake difference plot of MED1 (50-660) in free and bound to VDR-RXR-  
11 DNA states after 0.5, 2, 10 and 30 minutes of deuterations. Framed peptides represent the  
12 most impacted regions of MED1 (50-660) upon VDR-RXR-DNA binding presenting a statistical  
13 significance ( $p < 0.01$ , Wald Test, MEMHDX software) for the magnitude of the difference.  
14 Among them, blue highlighted peptides present RFU differences above 5% of RFU while grey  
15 highlighted peptides present RFU differences below 5% of RFU.

16  
17 **Supplementary Figure 12.** VDR-RXR-DNA-MED1 crosslink experiment. **(a)** Table summarizing  
18 all identified crosslinked sites (inter and intra) for the two used crosslinking agents.  $\text{C}\alpha$ - $\text{C}\alpha$   
19 distances are indicated for all identified VDR-RXR inter crosslinked peptides and where no  
20 distance was observed over the cut-off distance of each crosslinker (26-30Å and 20-24Å for  
21 DSBU and C2-arm version respectively). **(b)**  $\text{C}\alpha$ - $\text{C}\alpha$  distances for inter VDR-RXR identified  
22 crosslinks are represented on the heterodimer PyMOL structure.